The Astrophysical Journal, 598:858–877, 2003 December 1

Lyα EMISSION IN STARBURSTS: IMPLICATIONS FOR GALAXIES AT HIGH REDSHIFT[1]

J. M. Mas-Hesse[2]
Centro de Astrobiología (CSIC-INTA), Madrid, Spain; mm@laeff.esa.es

D. Kunth
Institut d'Astrophysique, Paris, France; kunth@iap.fr

G. Tenorio-Tagle
Instituto Nacional de Astrofísica, Óptica, y Electrónica, Puebla, Mexico; gtt@inaoep.mx

C. Leitherer
Space Telescope Science Institute, Baltimore, MD 21218; leitherer@stsci.edu

R. J. Terlevich[3]
Instituto Nacional de Astrofísica, Óptica, y Electrónica, Puebla, Mexico; rjt@inaoep.mx

and

E. Terlevich
Instituto Nacional de Astrofísica, Óptica, y Electrónica, Puebla, Mexico; eterlevi@inaoep.mx
Received 2003 March 13; accepted 2003 August 1

ABSTRACT

We present the results of a high-resolution UV two-dimensional spectroscopic survey of star-forming galaxies observed with *Hubble Space Telescope* Space Telescope Imaging Spectrograph. Our main aim is to map the Lyα profiles to learn about the gas kinematics and its relation with the escape of Lyα photons and to detect extended Lyα emission due to scattering in gaseous halos. We have combined our data with previously obtained UV spectroscopy on three other star-forming galaxies. We find that the P Cygni profile is spatially extended, smooth, and spans several kiloparsecs covering a region much larger than the starburst itself. We propose a scenario whereby an expanding supershell is generated by the interaction of the combined stellar winds and supernova ejecta from the young starbursts, with an extended low-density halo. The variety of observed Lyα profiles both in our sample and in high-redshift starbursts is explained as phases in the time evolution of the supershell expanding into the disk and halo of the host galaxy. The observed shapes, widths, and velocities are in excellent agreement with the supershell scenario predictions and represent a time sequence. We confirm that among the many intrinsic parameters of a star-forming region that can affect the properties of the observed Lyα profiles, velocity and density distributions of neutral gas along the line of sight are by far the dominant ones, while the amount of dust will determine the intensity of the emission line, if any.

Subject headings: galaxies: halos — galaxies: high-redshift — galaxies: ISM — galaxies: starburst — ISM: bubbles — ultraviolet: galaxies

On-line material: color figures

1. INTRODUCTION

Galaxies with ongoing star formation display characteristic emission lines whose strength often dominates the appearance of the optical spectrum (Kennicutt, Kobulnicky, & Pizagno 1998). The ionizing radiation from newly formed stars and its interaction with the surrounding gas generate collisionally excited and recombination lines, which become detectable at the highest observable redshifts (Melnick, Terlevich, & Terlevich 2000). Model spectra of young populations predict Lyα to be the strongest emission line in the optical/near-infrared (IR) spectral range for the simplified assumption of Case B recombination and low metal content (see Schaerer [2002] for a very recent set of model calculations). Therefore, Partridge & Peebles (1967) suggested the Lyα line as an important spectral signature in young galaxies at high redshift since the expected Lyα luminosity could amount to a few percent of the total galaxy luminosity.

Typical Lyα fluxes of 10^{-15} ergs s^{-1} cm^{-2} are expected for galaxies at redshifts around 3 with star formation rates of order $10^2\ M_\odot\ \mathrm{yr}^{-1}$. Such values have been within the reach of even relatively modest-sized instruments for several decades. Major observational efforts were undertaken to search for Lyα emission from such galaxies (Djorgovski & Thompson 1992). Although quite a few Lyα emitters powered by starbursts have been found (e.g., Kudritzki et al. 2000; Rhoads et al. 2000), their numbers are generally much lower than expected from the observed star-formation rates and Case B recombination conditions.

The assumption of the Lyα intensity as produced by pure recombination in a gaseous medium may be too simple. Meier & Terlevich (1981), Hartmann et al. (1988), Neufeld (1990), and Charlot & Fall (1993) considered the effects of

[1] Based on observations with the NASA/ESA *Hubble Space Telescope*, obtained at the Space Telescope Science Institute, which is operated by the Association of universities for Research in Astronomy, Inc., under NASA contract NAS5-26555.

[2] Laboratorio de Astrofísica y Física Fundamental-INTA, Madrid, Spain.

[3] Institute of Astronomy, Cambridge, UK.

dust on Lyα. Lyα photons experience a large number of resonant scatterings in neutral atomic hydrogen, thereby increasing the path length and the likelihood of dust scattering and absorption. This process can be very efficient in removing Lyα photons from the line of sight to the observer, leading to much lower line strengths in comparison with the idealized Case B. Depending on the aspect angle of the galaxy as seen from the observer, this may lead to a decrease of the Lyα equivalent width. On the other hand, Lyα may actually be enhanced because of the presence of many supernova remnants, which form during the starburst (Shull & Silk 1979). The net result is controversial. Bithell (1991) finds supernova remnants to be an important contributor to the Lyα strength, whereas Charlot & Fall (1993) reach the opposite conclusion.

The theoretical situation is sufficiently complex that observational tests are required. The most obvious test is measurement of Lyα in local starburst galaxies whose redshifts are sufficiently large to permit observations of their intrinsic Lyα outside the geocoronal and Galactic interstellar Lyα. Observations of local starbursts have indeed been performed with the *International Ultraviolet Explorer* (*IUE*) satellite (Meier & Terlevich 1981; Hartmann et al. 1988; Calzetti & Kinney 1992; Terlevich et al. 1993; Valls-Gabaud 1993). Again, the results are controversial. For instance, Calzetti & Kinney and Valls-Gabaud find Lyα strengths in agreement with pure recombination theory, whereas Hartmann et al. and Terlevich et al. conclude that significant dust trapping of Lyα photons must occur.

The superior spectral and spatial resolution of ultraviolet (UV) spectrographs on the *Hubble Space Telescope* (*HST*) has allowed new insight into the formation process of Lyα. *HST* Goddard High Resolution Spectrograph (GHRS) spectroscopy of eight gas-rich irregular galaxies by Kunth et al. (1998) indicates yet another, and most likely the dominant, parameter governing Lyα emission: neutral gas kinematics. Kunth et al. found Lyα emission with blueshifted absorption in four of the galaxies. In these objects the O I and Si II absorption lines are also blueshifted, suggesting an outflow of the neutral gas with velocities around 200 km s^{-1}. The other four galaxies show broad damped Lyα absorption profiles centered on the wavelength of the ionized gas, with no detection of Lyα emission. The observed galaxies span a metallicity range of more than a factor of 10 and display no correlation between metal abundance and Lyα emission strength, a correlation that had been postulated on the basis of the *IUE* spectra and on theoretical grounds because of the appearance of dust. The velocity structure of the neutral gas in these galaxies is the driving factor that determines the detectability of Lyα in emission. When most of the neutral gas is velocity-shifted relative to the ionized regions, the Lyα photons can escape, a suggestion supported by recent models of Tenorio-Tagle et al. (1999). Nevertheless, while the velocity structure of the neutral gas is the driver for the detectability of the Lyα emission, we want to stress that the amount of dust will still be responsible for the *intensity* of the line, when observed. The Lyα photons not affected by resonant scattering will still be strongly affected by dust extinction, which has a maximum in the UV range, around the Lyα wavelength. The properties of the neutral gas (density, kinematics, and covering factor) thus determine the shape of the profile and the equivalent width of the line, while the amount of dust drives only its intensity. The implication is that feedback from the massive stars via ionization and the creation of superbubbles and galactic-scale outflows lead to the large variety of Lyα profiles. The escape of Lyα photons depends critically on the column density of the neutral gas and dust, the morphology of the supershells, and the kinematics of the medium. Since these effects can be highly stochastic, theoretical predictions for the Lyα strength are quite uncertain, and empirical guidelines are called for.

A similar pattern seems to apply to high-redshift galaxies. At $2.5 < z < 5.2$, about half of the galaxies found show Lyα in emission (Steidel et al. 1999; Rhoads et al. 2000; Frye, Broadhurst, & Benítez 2002). At the same time, the Lyα line is asymmetric, displaying an extension toward larger wavelengths. The blue "edge" of the line could be described as showing a P Cygni profile, and the centroid of the line is redshifted by several hundred km s^{-1} with respect to the metallic absorption lines. This is consistent with gas outflows, breakout of the gas bubble produced by the star-forming region, and results in the escape of Lyα emission.

In order to analyze the spatial (kinematical) structure of the Lyα emission in nearby star-forming galaxies, we used the Space Telescope Imaging Spectrograph (STIS) on board *HST* to reobserve three galaxies of the Kunth et al. (1998) sample, two of which clearly showed with GHRS a P Cygni Lyα profile (Haro 2 and IRAS 0833+6517) and the third of which presented only a broad Lyα absorption (I Zw 18). We aimed also to analyze whether Lyα could be leaking in external regions while being completely absorbed around the starburst itself.

The data and data analysis technique are presented in § 2, the expected structure of an H II region and subsequent effects on the resulting Lyα profiles follow in § 3, and the superbubble generated by the H II region and their time evolution are analyzed in § 4, together with the expected effect on the observed Lyα line profile. The general discussion is presented in § 5, and the particular implications for high-redshift galaxies are presented in § 6. Finally, § 7 of the paper presents the summary and conclusions of our work.

2. *HST*/STIS OBSERVATIONS

We list in Table 1 the basic data for the galaxies observed with *HST*/STIS. The journal of observations is summarized in Table 2. We will complement our discussion with some data presented by Thuan & Izotov (1997). These authors analyzed a sample of three compact galaxies experiencing strong starbursts. They found Lyα emission in only one case, Tol 1214−277. The line was very strong and rather symmetric, with no evidence of blueshifted absorption. They concluded that in this case the line was visible because the covering factor of the neutral cloud was small, leaving Lyα photons able to escape through paths relatively free of H I gas.

Previous GHRS spectra were taken through the Large Science Aperture (LSA), comprising roughly $1\farcs7 \times 1\farcs7$ ($2'' \times 2''$ for the pre-Costar I Zw 18 data), centered on the maximum UV continuum. STIS data have been obtained through the $52'' \times 0\farcs5$ slit on the FUV MAMA and optical CCD detectors.

In the FUV range the G140M grating was used. The data have been extracted with standard STSDAS procedures. The different integrations obtained were combined and averaged with the *mscombine* task to improve the signal-to-noise ratio. The detector and geocoronal background

TABLE 1
PROPERTIES OF THE OBSERVED H II GALAXIES

Object	R.A. (2000.0)	Decl. (2000.0)	$M(B)$	v(hel) (km s^{-1})	Distance (Mpc)	Scale (pc arcsec^{-1})	12+log(O/H)
IRAS 0833+6517	08 38 23.2	65 07 15	−20.8	5730	85.4	413	7.5[a]
I Zw 18	09 34 02.4	55 14 32	−14.0	780	10	48.4	7.2[b]
Haro 2	10 32 31.9	54 24 03	−18.2	1461	19.5	94.4	8.4[c]

NOTE.—Adopted properties of the observed H II galaxies are taken from the NASA Extragalactic Database, except for the metallicity, for which the references are indicated. Units of right ascension are hours, minutes, and seconds, and units of declination are degrees, arcminutes, and arcseconds.
[a] Margon et al. 1988.
[b] Skillman & Kennicutt 1993.
[c] Davidge 1989.

was removed, averaging 100 rows on areas below and above the stellar continuum. While the detector background was negligible for Haro 2 and IRAS 0833+6517, it affected significantly the bluest continuum of I Zw 18.

Low-resolution optical spectra were taken with the STIS CCD using the G430L grating in order to compare locally the extension and intensity of Lyα and optical emission lines, namely, [O II], [O III], and Hβ. The optical spectrum of I Zw 18 was underexposed, but we could clearly detect the extension of the optical lines for Haro 2 and IRAS 0833+6517.

The UV spectral images have a spatial scale of 0.″029 and a spectral dispersion of 0.053 Å pixel^{-1}, giving a spectral resolution around 0.15 Å, translating to ∼37 km s^{-1} at the Lyα wavelength. The optical images have corresponding scales of 0.″05 and spectral dispersion of 2.7 Å pixel^{-1} (spectral resolution ∼6.7 Å). We have multiplied the resulting fluxes by the STIS parameter *diff2pt* (diffuse to point-source conversion factor for absolute photometry), as required for nonextended sources—although resolved, the objects are indeed rather compact.

In the next section we describe in detail the observations object by object.

2.1. *Haro 2*

We show in Figure 1 the STIS spectral image of Haro 2 with different scales. The slit is oriented along the minor axis of the galaxy (during a first observation with the slit along the major axis the aperture was unfortunately misplaced as the result of an observer error). It can be seen that the UV continuum is very compact, extending over only around 0.″9 (corresponding to ∼85 pc). There is a very strong, quite extended, and spatially asymmetric Lyα emission line. Lyα emission is detected over 7″, 6″ of which are located to the upper (southwest) part of the slit. There are hints that the nebulosity is even more extended, at a fainter level, to this direction. The peak of the Lyα emission is slightly offset (by 0.″2, or 19 pc) from the peak of the UV continuum. A spatial profile of the Lyα emission and the UV continuum is shown in Figure 2. In Figure 3 we display the extracted spectrum of the central region of this galaxy.

The most striking result from these data is that the conspicuous and completely black absorption edge affects the blue wing of the Lyα profile over the whole region where Lyα is detected, at essentially the same velocity. This implies that the neutral gas that causes the resonant scattering is approaching us at around 200 km s^{-1} and extends over at least ∼8″(∼750 pc), with no hint of any velocity structure. We show in Figure 4 the Lyα profile at different positions over the slit. The zero in the velocity scale corresponds to the Lyα centered at the redshift of the central H II region determined from the optical emission lines. These plots confirm that the blue edge of the Lyα profile always appears at basically the same velocity, with variations smaller than ±30 km s^{-1}. Note as well that the red wing of the Lyα emission profile extends essentially to the same velocity (∼+500 km s^{-1}) all along the slit, independently of the peak intensity of the line. As we will discuss later, the emission from this wing originates from a receding shell far from the central H II region.

TABLE 2
JOURNAL OF OBSERVATIONS FOR THE *HST* PROPOSAL 8302

Object	Observation Date	Grating	Integration time (s)	Position Angle (deg)	R.A. (deg)	Decl. (deg)
IRAS 0833+6517	2001 Jan 15	G430L	360	171	129.59666	65.12083
IRAS 0833+6517	2001 Jan 15	G140M	1320, 3000, 3000	171	129.59666	65.12083
I Zw 18	2000 Oct 4	G430L	300	−96	143.50833	55.24094
I Zw 18	2000 Oct 4	G140M	1764, 3135, 3089, 3089	−96	143.50833	55.24094
Haro 2 no. 1[a] (major axis)	2000 Feb 21	G430L	300	150	158.13250	54.40972
Haro 2 no. 1[a]	2000 Feb 21	G140M	1724, 3111, 3065	150	158.13250	54.40972
Haro 2 no. 2 (minor axis)	2000 Dec 1	G430L	300	−121	158.13250	54.40097
Haro 2 no. 2	2000 Dec 1	G140M	1724, 3111, 3065	−121	158.13250	54.40097

NOTES.—The 52 × 0.5 slit was used in all cases. The UV spectra were obtained with the FUV-MAMA detector, at a central wavelength of 1222 Å. The optical spectra were obtained with the CCD, at a central wavelength of 4300 Å. The position angle of the Y-axis is measured in degrees east of north. The coordinates indicated correspond to the center of the slit, as extracted from the STIS files headers (J2000.0).
[a] Because of an error, the center of the slit was misplaced 31″ to the north during this visit.

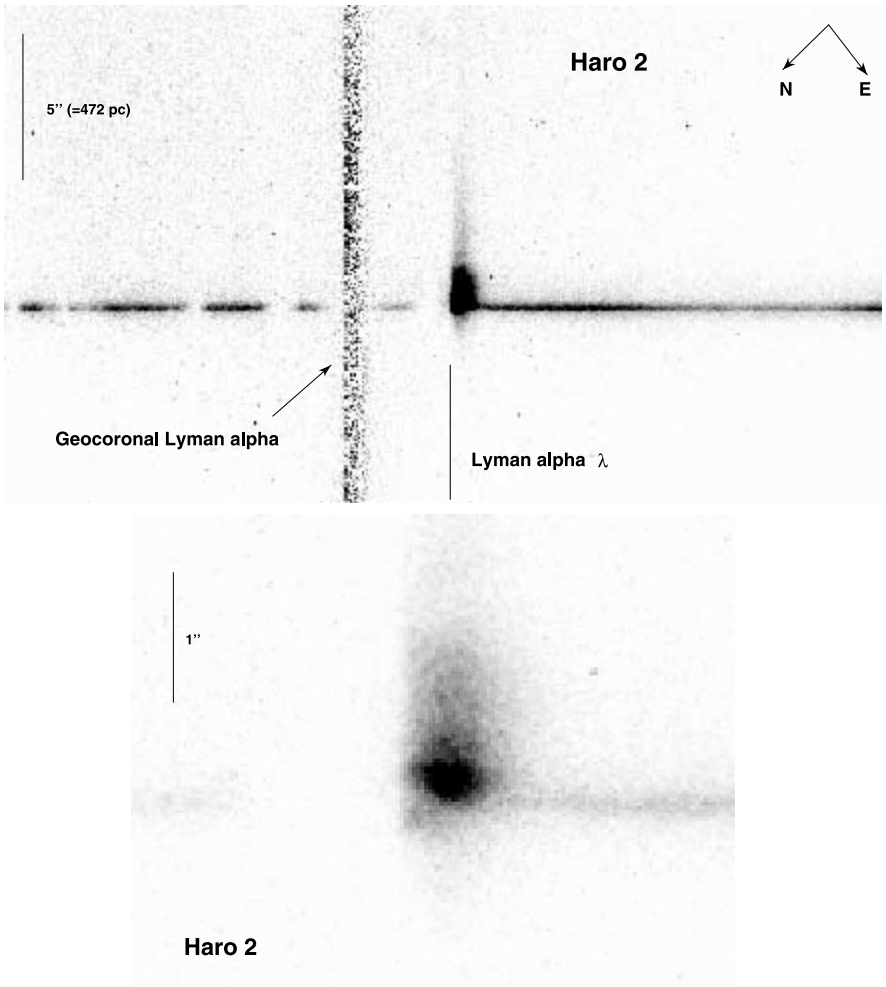

FIG. 1.—UV spectral images of Haro 2. *Top:* We have marked the position of the geocoronal Lyα line residuals, after background subtraction. The vertical line marks the expected position of the Lyα wavelength at the redshift derived from the H II region. The pixels have been rebinned for better display. We show the angular scale along the spatial axis, as well as the corresponding spatial scale. The north and east arrows indicate the orientation of the slit on the sky. *Bottom:* Detail of the Lyα region. The image cuts have been selected to show the structure of the Lyα emission. The displayed pixels correspond to physical detector pixels. The wavelength scale increases to the right on the *X*-axis.

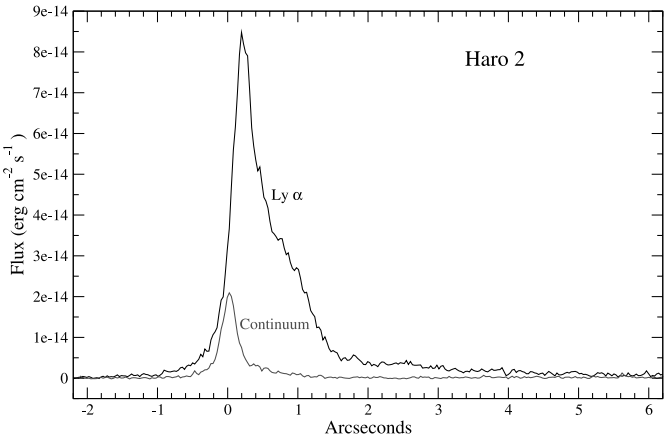

FIG. 2.—Spatial profile of the Lyα line in Haro 2 on top of the UV continuum profile. Note the Lyα emission extended to the southwest (to the right in the plot), with almost no counterpart on the UV continuum. [*See the electronic edition of the Journal for a color version of this figure*.]

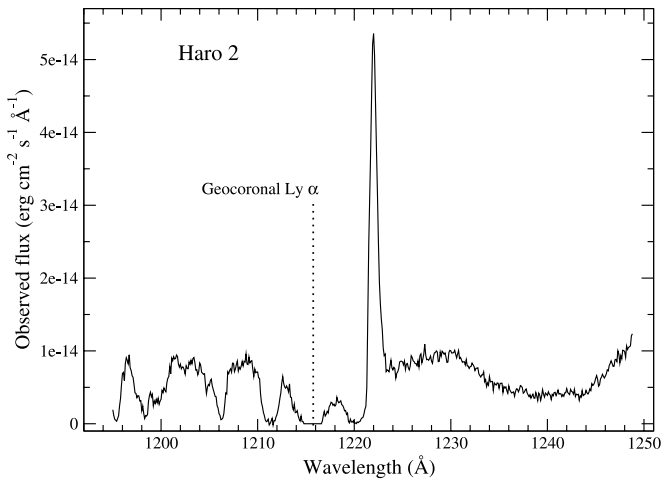

FIG. 3.—Extracted spectrum of the central region of Haro 2 (corresponding to 0$''$.4). The position of the geocoronal Lyα line has been marked. Several interstellar absorption lines are detected blueward of the Galactic Lyα line. Note the broad but weak apparent absorption centered around 1240 Å, of unknown origin.

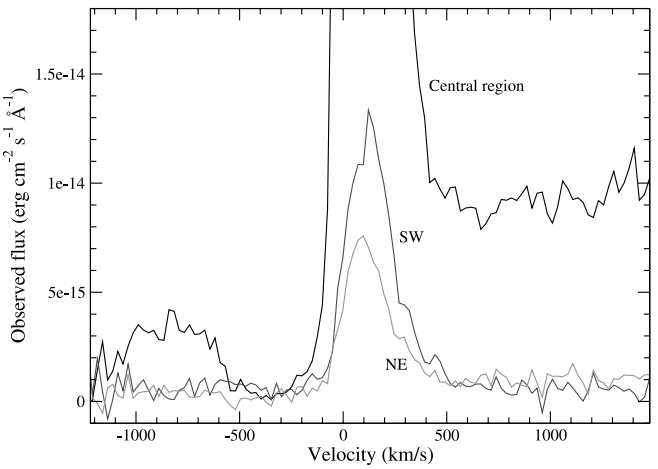

FIG. 4.—Lyα emission-line spectral profiles in different regions of Haro 2. *Strongest profile:* central region. *Intermediate profile:* extended emission integrated over a region of 1″.5 centered 2″.3 southwest of the nucleus. *Weakest profile:* extended emission over 0″.7 centered at 0″.8 northeast of the nucleus. Note that the profiles red wing vanishes always at around 500 km s^{-1}, independently of the strength of the line. Similarly, the blue wing goes to zero at around -200 km s^{-1} in the three regions. [*See the electronic edition of the Journal for a color version of this figure.*]

The optical spectral image is shown in Figure 5. The optical continuum, from 3000 to 5000 Å, is very blue and appears to be dominated by very young stars, as illustrated in Figure 6. The already known Wolf-Rayet feature at around 4686 Å is clearly detected in the spectrum. Emission lines are detected over an extent of $\sim$1″.5, which corresponds to the core of the Lyα line. The optical lines show some asymmetry at the upper part of the slit. The spectrum has enough signal-to-noise ratio to measure the total flux of Hβ and the O II+O III lines; these are listed in Table 3, together with the Lyα flux. It is important to note that these fluxes are integrated over the same area (1″.5 $\times$ 0″.5), and hence their ratios reflect the intrinsic local ratios in the gas. The observed Lyα/Hβ ratio is only $\sim$2.1, much below the theoretical value Lyα/H$\beta \sim 33$. Mas-Hesse & Kunth (1999) measured an extinction of $E(B-V) = 0.22$, as derived from the Balmer lines observed through a rather large aperture containing the whole ionized region. With this extinction, the expected Lyα/Hβ ratio would be around 3.4 (assuming a Large Magellanic Cloud [LMC] extinction law in the UV; see Mas-Hesse & Kunth 1999). This implies that the effect of resonant scattering has lowered the Lyα intensity by at least 40%. Nevertheless, we stress that this extinction value

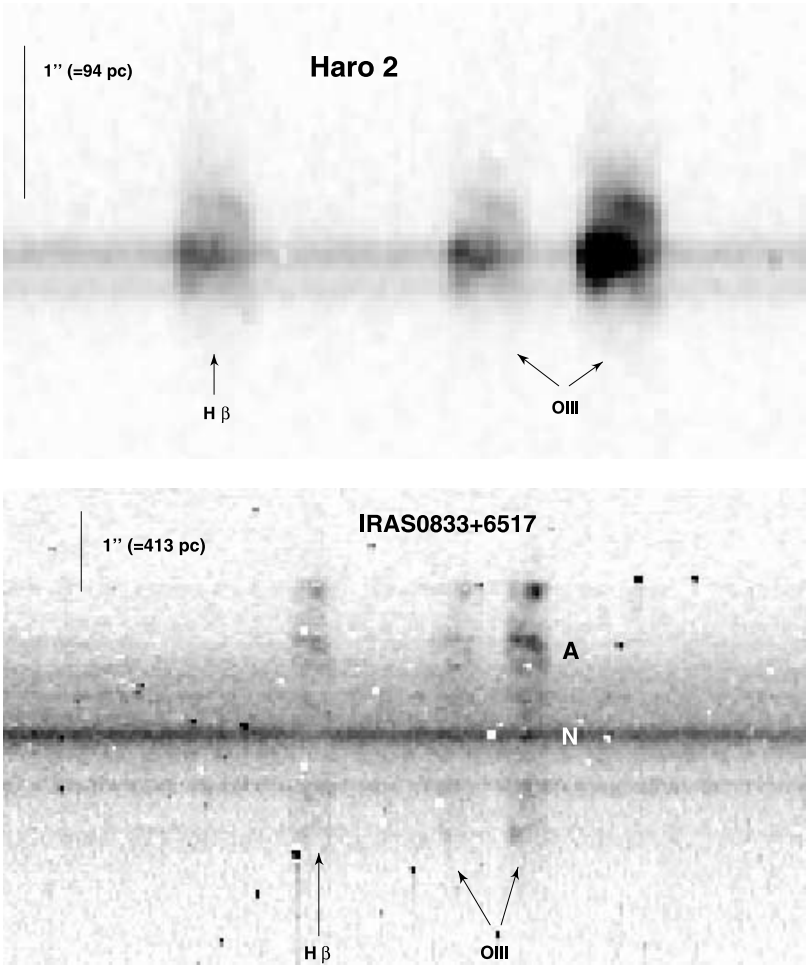

FIG. 5.—Optical spectral images: Haro 2 (*top*) and IRAS 0833+6517 (*bottom*). The position of the Hβ and O III lines has been marked, as well as the angular and spatial scales along the *Y*-axis. The pixels displayed correspond to physical detector pixels. Some velocity structure is apparent in the O III lines on the Haro 2 image. The velocity shift between both peaks corresponds to around 700 km s^{-1}. Such velocity offsets have not been detected on the Lyα emission line. In the bottom panel we have marked with "A" and "N" the regions for which we have extracted the spectra shown in Fig. 11. Dark and white pixels are the residuals of regions affected by cosmic-ray hits.

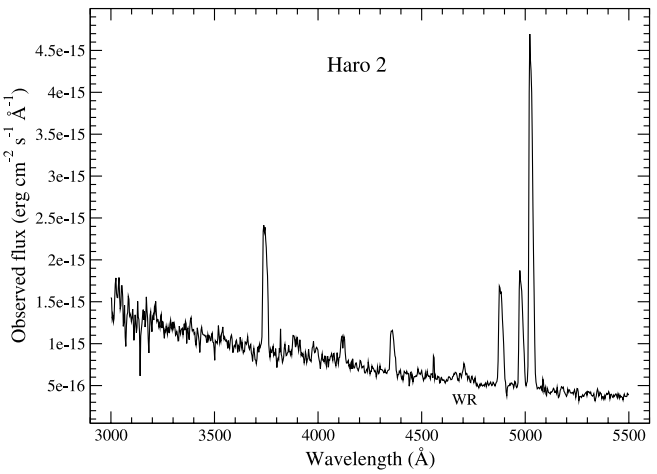

FIG. 6.—Optical spectrum of Haro 2, integrated over an aperture of 0″.3. Note the Wolf-Rayet feature at around 4686 Å.

represents an average over a large region. Since the Balmer line ratio is not measured with the same spatial resolution as the Lyα line, it is not possible to disentangle effects due to dust extinction from those of resonant scattering.

This galaxy exemplifies the paradigm defining the detectability of the Lyα emission line: while most of the line emission has been destroyed in this case by dust absorption, the line is still detectable, and indeed is quite prominent, because of the kinematical configuration of the neutral gas surrounding the H II region. If there were no dust at all, the line would remain undetectable unless the neutral gas were expanding. On the other hand, if there were not neutral gas at all, both the Lyα emission line and the surrounding continuum would experience roughly the same absorption, so that the equivalent width of the line would remain unaffected, independently of the amount of dust. Only the absolute line intensity would be strongly dependent on the presence of dust.

The evolutionary synthesis modeling by Mas-Hesse & Kunth (1999) yielded an age for the starburst episode around 4.8 Myr and more than $6.6 \times 10^6\ M_\odot$ of gas having been transformed into stars. As cited by these authors, there is evidence in Haro 2 of previous recent starburst episodes, which could have taken place in the last 50 Myr.

TABLE 3
SUMMARY OF OBSERVATIONAL RESULTS

Parameter	IRAS 0833+6517	Haro 2
F[O II] λ3727	6.0e-14	1.2e-13
F[O III] λ4959	2.3e-14	6.9e-14
F[O III] λ5009	6.5e-14	2.0e-13
F(Hβ).....	2.0e-14	7.7e-14
W(Hβ) (Å)	8	75
F(Lyα)	4.3e-14	1.6e-13
W(Lyα) (Å).....	6	12
F(sec. Lyα).....	4.0e-15	...
Aperture	3″.5 × 0″.5	1″.5 × 0″.5

NOTES.—The emission-lines intensities have been measured through the same apertures in the UV and optical, so that their ratios reflect the intrinsic ratios in the gas. Lyα has been measured extrapolating the UV continuum from longer wavelengths. The fluxes are given in units of ergs s^{-1} cm^{-2}.

2.2. *IRAS 0833+6517*

The STIS spectral images of IRAS 0833+6517 reveal a much more complex structure than Haro 2 (see Fig. 7). The UV continuum shows a patchy distribution and is extended over ∼3″ (1.2 kpc)—its limits are diffuse: the UV continuum seems to be even more extended at a lower brightness level. There is also a strong, quite extended, and spatially asymmetric Lyα emission line. Lyα emission is detected over at least ∼10″ (4.1 kpc). Lyα emission shows two main peaks. The brightest is slightly offset with respect to the center of the UV emission, ∼0″.3 (124 pc) to the upper (south) part of the slit. The second peak is also offset, ∼1″.2 (496 pc) to the lower (north) part of the UV continuum. Some weaker peaks can also be identified on the image. This is shown in Figure 8, where we plot the spatial profile of the Lyα emission, on top of the continuum profile. The extracted spectrum in the Lyα region is given in Figure 9, showing the asymmetric Lyα emission line with a broad absorption to the blue.

We show in Figure 10 the Lyα emission profile across different regions. As already found in Haro 2, the blue absorption edge has no significant velocity structure over at least the 10″ (4.1 kpc) along the slit where emission is detected (the velocity at which the profiles go to zero in the different regions is within the range −50 to +50 km s^{-1}. Here again, the neutral gas in front of the H II region, within at least 4.1 kpc, is approaching us at basically the same velocity, ∼300 km s^{-1}. Moreover, the red wing of the emission profile extends to roughly the same velocity, around 700 km s^{-1}, as also found on Haro 2.

We confirm the detection made on the GHRS spectrum of a secondary Lyα emission line, blueshifted by around −300 km s^{-1} with respect to the H II region velocity determined from the optical emission lines. This secondary emission shows some interesting features:

1. It is clearly offset from the continuum, peaking at ∼0″.9 (370 pc) from the UV continuum, to the upper (south) part of the slit. The emission, at a weaker level, extends clearly to the lower (north) part of the slit, at least over the region where there is some UV continuum.
2. Although the signal-to-noise ratio is low, this secondary emission peak shows some velocity structure, with components redshifted by ∼100 km s^{-1} from its average centroid. In general, the profile is not a Gaussian one and seems to be the convolution of various emissions at different velocities.

We show in Figure 5 the spectral image of IRAS 0833+6517 taken in the optical range. The continuum has a narrow peak about ∼0″.3 wide (124 pc), on top of a weaker extension over ∼2″(826 pc). There is a region to the upper part of the slit that is clearly more conspicuous in the UV than in the optical. It is here where Lyα and the forbidden oxygen lines peak. This region is offset by ∼1″.2 (496 pc) from the optical continuum maximum. We show in Figure 11 the optical spectra of the bright nucleus and of this region.

We believe that the maximum of the optical continuum is due to relatively older stars, with a weak contribution to the UV and to the ionization. Indeed, coincident with the

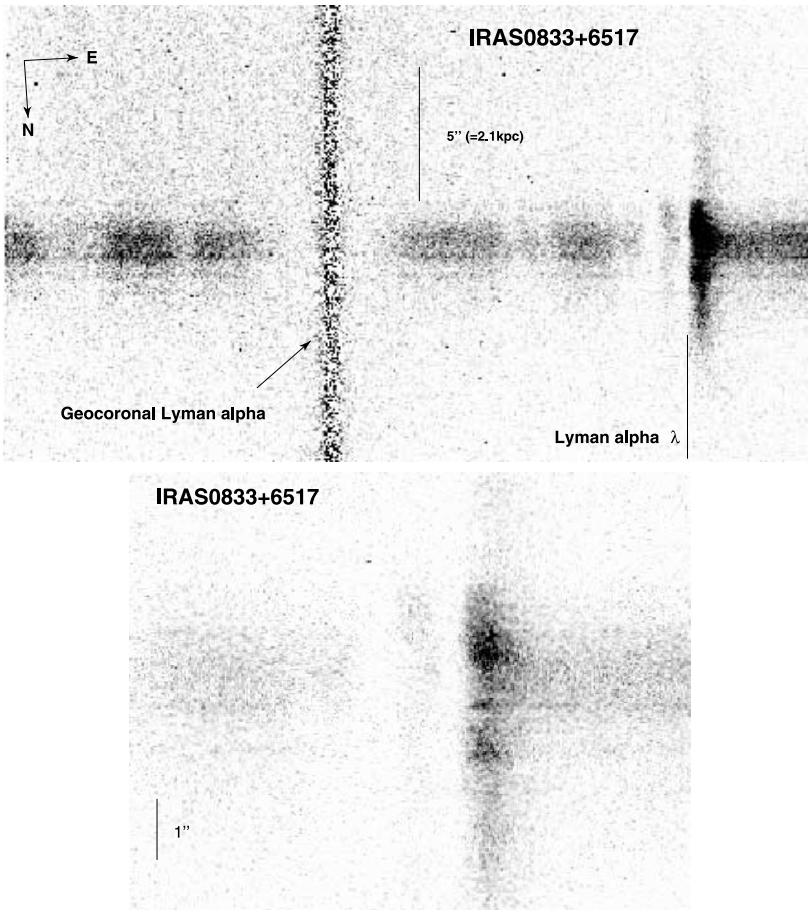

FIG. 7.—UV spectral images of IRAS 0833+6517. *Top:* We have marked the position of the geocoronal Lyα line residuals, after background subtraction. The vertical line marks the expected position of the Lyα wavelength at the redshift derived from the H II region. The pixels have been rebinned for better display. We show the angular scale along the spatial axis, as well as the corresponding spatial scale. The north and east arrows indicate the orientation of the slit on the sky. *Bottom:* Detail of the Lyα region. The image cuts have been selected to show the structure of the Lyα emission. The displayed pixels correspond to physical detector pixels. The wavelength scale increases to the right on the *X*-axis. The extracted spectrum is shown in Fig. 9.

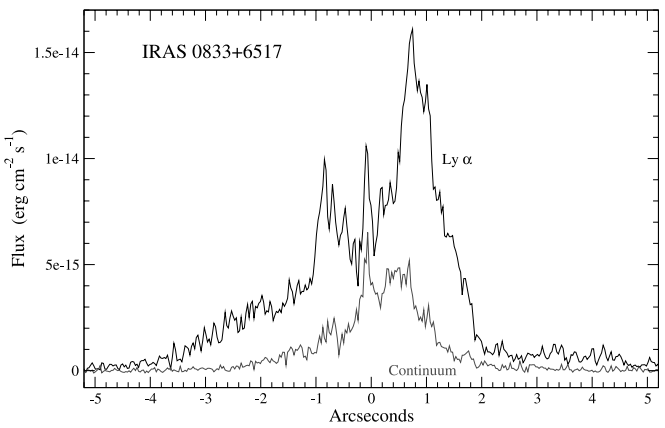

FIG. 8.—Spatial profile of the Lyα line in IRAS 0833+6517 on top of the UV continuum profile. The regions with the strongest Lyα emission are not correlated with the location of the strongest UV continuum sources. [*See the electronic edition of the Journal for a color version of this figure*.]

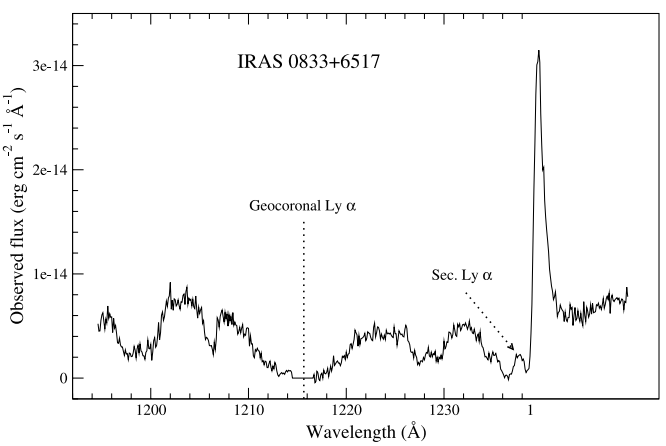

FIG. 9.—Extracted spectrum of the central region of IRAS 0833+6517 (corresponding to 2.″0). The position of the geocoronal Lyα line has been marked, in the center of the broad Galactic absorption profile. We have also marked the position of the secondary emission peak, whose spatial distribution can be appreciated in Fig. 7. Note the splitting of the Si III λ1206 absorption line, with peaks at 1227 and 1229 Å. Additional broad interstellar absorption lines are detected blueward of the Galactic Lyα line.

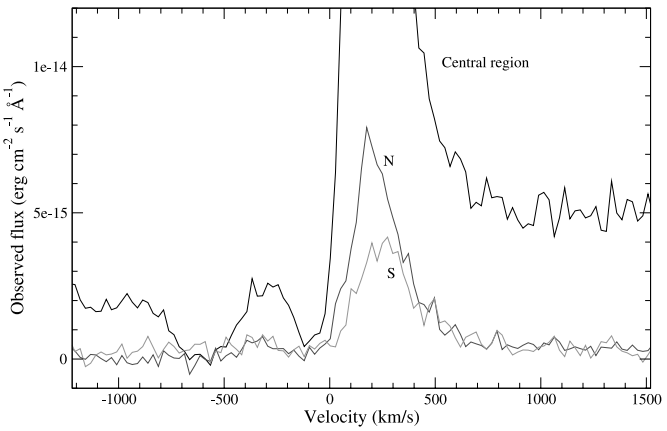

FIG. 10.—Lyα emission-line spectral profiles in different IRAS 0833+6517 regions. *Strongest profile:* central region. *Intermediate profile:* extended emission integrated over a region of 2″.3 centered 3″.0 N of the nucleus. *Weakest profile:* extended emission over 4″.1 centered at 3″.0 south of the nucleus. Note again that the profiles extend over basically the same velocity range independently of their strength. The secondary emission profile, centered at −300 km s^{-1} appears only in the central region. [*See the electronic edition of the Journal for a color version of this figure.*]

optical continuum maximum there is a local minimum in all emission lines strengths. The optical continuum shows a very prominent Balmer decrement, as well as Balmer absorption lines of stellar origin, but only in the central region (see Fig. 11). The optical continuum in the upper part, where the emission lines peak, is much bluer and has weaker Balmer decrement and Balmer stellar absorptions, as shown on the figure. González Delgado et al. (1998) presented a detailed analysis of the massive young stellar population in this galaxy based on evolutionary synthesis models. They derived a relatively old age for the burst between around 6 and 7 Myr. These authors concluded that there was a significant dilution by an underlying older stellar population, which we identify indeed with the population producing the maximum of the optical continuum.

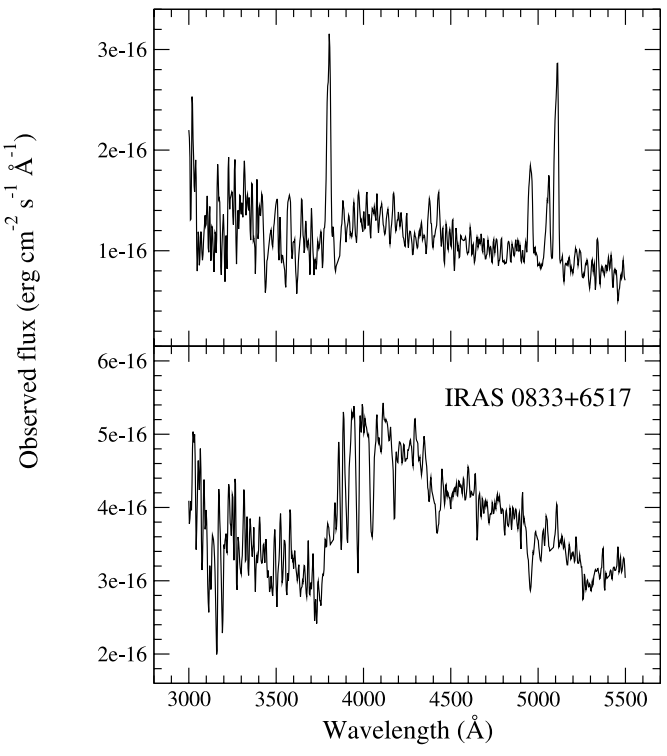

FIG. 11.—Extracted optical spectra of IRAS 0833+6517 for the regions marked in Fig. 5: the "A" region is the top panel, and the "N" region is the bottom one.

Finally, [O II], [O III], and Hβ are detected over ∼3″.5 (1.4 kpc) and coincide again with the core of the Lyα emission. The measured Lyα/Hβ ratio is ∼2.1, indeed similar to the value measured in Haro 2 (see Table 3). González Delgado et al. (1998) quote a large range of extinction values for this galaxy, with $E(B-V)$ between 0.17 and 0.52. According to these authors, the value derived from the Balmer lines ratio is $E(B-V) = 0.52$. Assuming this extinction and an LMC law, the expected Lyα/Hβ ratio would be only around 0.28, much smaller than the value measured by us. On the other hand, if we consider the extinction value derived from the continuum fits, with $E(B-V) = 0.17$, and the same LMC law, the expected ratio would be much higher, Lyα/Hβ ∼ 7, indeed significantly higher than the measured value. We conclude again that although the effects of extinction and scattering cannot be disentangled, our results show clearly that both effects must significantly affect the observed properties of the Lyα emission line.

2.3. *I Zw 18*

We show in Figure 12 the STIS UV spectral image of I Zw 18. The UV continuum is quite extended (over ∼2″, corresponding to ∼97 pc). The total flux within the STIS aperture is around a factor 4 lower than within the GHRS aperture (2″ × 2″, pre-Costar data), which is consistent considering the extension of the source.

A very broad and damped Lyα absorption is detected, with complete blackening at the center of the line, as shown in Figure 13. The longer wavelength range of STIS allows for a more complete coverage of the absorption red wing, as compared to the GHRS data from Kunth et al. (1998), confirming the properties of the damped absorption profile reported there. No emission is seen at any position along the slit, regardless the intensity of the continuum. This is clearly understood if the neutral gas covers the whole ionized region with a large column density. This neutral gas must be static with respect to the central H II region all along the region covered by the slit, so that resonant scattering affects all Lyα photon emitted by the central H II region. The complete blackening of the absorption profile indicates that essentially all photons have been finally destroyed, most likely by dust absorption.

3. THE STRUCTURE OF AN H II REGION AND EFFECTS ON THE RESULTING Lyα PROFILES

An H II region surrounding a cluster of massive newly formed stars should produce an intrinsic Lyα emission line with a Lyα/Hα ratio around 11 and an intrinsic velocity dispersion (σ) similar to the optical Balmer lines one. Nevertheless, there are several factors affecting significantly both the intensity and the profile of the Lyα line as observed from outside the H II region. We will discuss the different effects in this section aiming to explain the observed Lyα profiles.

The main effects contributing to modify the Lyα emission line are the following:

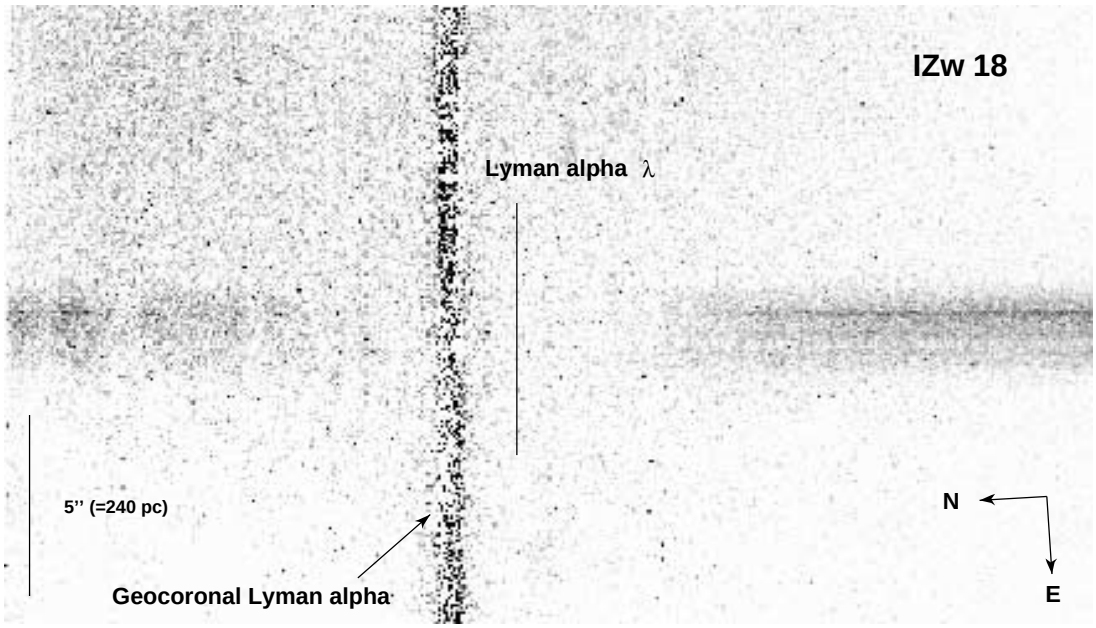

FIG. 12.—UV spectral image of I Zw 18. Symbols are as in Fig. 1. Note the broad damped absorption profile, blended with the Galactic absorption. Note also the lack of Lyα photons in emission along the slit.

1. *Absorption by dust*.—The known extinction curves peak in the far UV range (around 1000 Å), so that the interstellar extinction will be maximum around Lyα. As an example, an $E(B-V)$ of 0.2 will yield the absorption of 38% Hα luminosity, but of 96% of the Lyα emission—according to the Small Magellanic Cloud law, which is generally valid in these environments (Mas-Hesse & Kunth 1999).

As a first approximation, the Lyα line and the surrounding continuum should experience the same extinction by dust (assuming there is no neutral gas along the line of sight), so the equivalent width of the line would not be affected. Therefore, in regions where the continuum is well detected, dust absorption alone could not explain the weakness or even absence of Lyα in emission.

Nevertheless, recall that the spatial distribution of stellar continuum sources, ionized gas, and dust clouds might be very different, as found in nearby starburst galaxies (see, e.g., the analysis of NGC 4214 by Maíz et al. [1998]). This spatial decoupling might lead to very different extinctions affecting the UV continuum and the emission lines, as discussed by Mas-Hesse & Kunth (1999).

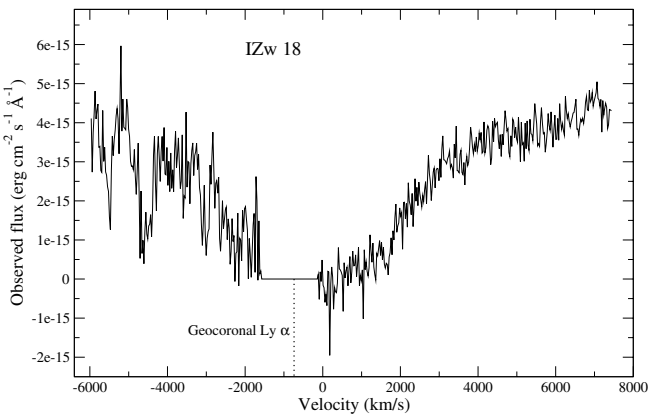

FIG. 13.—Extracted spectrum of the central region of I Zw 18 (corresponding to 2.″0). The abscissa axis is given in velocity scale to show the width of the absorption profile. Additional interstellar absorption lines are detected blueward of Lyα.

2. *Scattering by neutral hydrogen*.—Lyα photons traveling through neutral hydrogen will suffer resonant scattering, which will redistribute them within the cloud. This effect dramatically increases the sensitivity of Lyα photons to dust absorption. In the presence of neutral hydrogen we therefore expect the complete destruction of Lyα photons by dust absorption, even in environments with relatively low dust abundance.

3. *Presence of expanding shells*.—The presence of an expanding shell around the H II region can dramatically affect the shape and intensity of the Lyα emission line. We have identified four major elements:

a) If the expanding shell is sweeping the neutral gas, the resonant scattering will affect photons with energy slightly higher than those of the central Lyα emission line. As a result, only part of the Lyα emission will be able to go through the neutral medium and become visible. P Cygni–like profiles will be expected in these cases, as we will show later.

b) If a fraction of ionizing photons escapes the central H II region, the ionization front could reach the internal layers of the shell. We would expect to detect then a redshifted Lyα emission component originated at the inner surface of the receding shell.

c) In addition, part of the Lyα photons produced in the central H II region could be backscattered by the neutral layers of the receding shell to the observer's line of sight, appearing also redshifted (with respect to the H II region systemic velocity) by the shell expansion velocity.

d) Finally, a recombining region, behind the leading shock, could cause a secondary Lyα emission component, which would be observed blueshifted by the shell expansion velocity. Since this component originates *outside* the neutral

shell, it would not be affected by resonant scattering by the neutral layers.

In the next sections we will analyze in more detail the effects related to resonant scattering and the presence of an expanding shell.

3.1. *Effect of Resonant Scattering*

Neutral hydrogen will scatter resonantly the Lyα photons inside the cloud. In Figure 14 we show the expected absorption profiles produced by a layer of neutral hydrogen with different column densities. Profiles have been computed using the XVoigt code (Mar & Bailey 1995), assuming a thermal broadening of the neutral cloud with $b = 20$ km s^{-1}. The figure shows how huge the effects of resonant scattering by neutral hydrogen are: for relatively small column densities ($N \sim 10^{14}$ cm^{-2}), the center of the line reaches total absorption. For column densities higher than $N \sim 10^{18}$ cm^{-2}, the line becomes damped and the full saturation (hence no transmission) spreads rapidly toward both sides. Remark from the figure that for $N \sim 10^{21}$ cm^{-2} all photons emitted by particles within a range in velocity of ± 1000 km s^{-1} will be completely absorbed. This not only affects the Lyα emission-line photons, but also those photons from the surrounding continuum emitted by the central cluster of massive stars. Moreover, the wings of the absorption would affect photons at energies corresponding to more than ± 4000 km s^{-1} from the line center.

In principle, resonant scattering by neutral hydrogen does not destroy the incident Lyα photons. In a completely dust-free cloud, photons would be internally scattered until they reach the external surface of the cloud, from where they are able to escape. We would expect Lyα photons to leak from the overall surface of the neutral cloud surrounding the H II region, producing a very low surface brightness. Ahn, Lee, & Lee (2001, 2002) have discussed the effects of Lyα photons scattering by neutral hydrogen in a dustless and static medium. They assume that no photons are destroyed (in absence of dust) and then analyze the redistribution in frequencies of the escaping radiation. They predict the formation of a rather narrow absorption trough at the line center, with extended red and blue wings, but their profiles differ significantly from the observed ones, basically because the effect of dust was not considered in these works. Indeed, Kunth et al. (1998) showed that when a static cloud of neutral gas is surrounding the H II region, the resulting profile corresponds to a typical Voigt-like absorption line. We stress again that even very small amounts of dust completely destroy all scattered photons via multiple scattering events. Our simulations consider that all photons affected by scattering, according to the corresponding Voigt function, will be finally absorbed by dust and will not be reemitted.

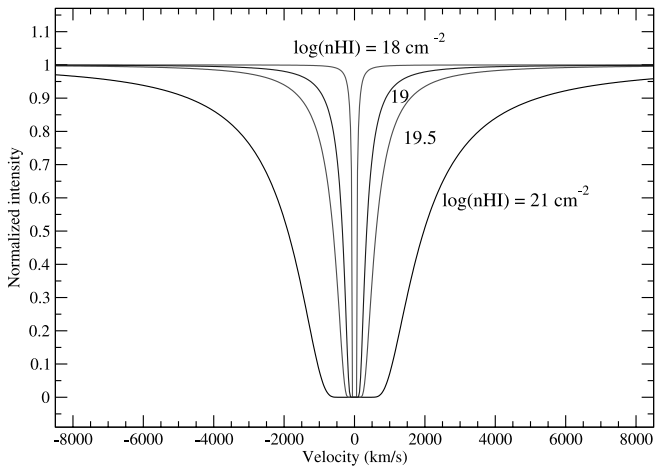

FIG. 14.—Voigtian absorption profiles computed for neutral hydrogen densities $\log n$ (H I) = 18, 19, 19.5 and 21 cm^{-2} (from weaker to stronger absorption). We have assumed $b = 20$ km s^{-1}. [*See the electronic edition of the Journal for a color version of this figure*.]

3.2. *Effects Caused by an Expanding Shell*

According to the profiles shown in Figure 14, it would become nearly impossible to detect Lyα in emission from starburst galaxies, since they are usually immersed in rather dense neutral clouds. However, we argue that the presence of an expanding shell, with properties evolving concurrently with the central cluster of massive stars, allows for an explanation of the various profiles actually detected in most objects, as discussed in Tenorio-Tagle et al. (1999). In the following discussion the expansion velocity of the shell, $v_{\rm exp}$, will refer to the velocity of the shell with respect to the central static H II region.

We first show in Figure 15 the expected Lyα profiles when the neutral gas surrounding the H II region is expanding at a certain velocity ($v_{\rm exp}$), for different H I column densities along the line of sight. As explained above, resonant scattering in the expanding neutral gas affects photons with higher energies than those emitted in the Lyα line by the central H II region. As a result, the absorption of Lyα photons mostly affects the blue wing of the emission profile, producing a classical P Cygni shape. The damped part of the absorption profile remains completely black, and the emission line becomes strongly asymmetric. If the H I column density is high enough (in our example, above around 10^{21} cm^{-2}), the absorption is total, and only a broad damped profile would be detected. The resulting spectrum will nevertheless depend on the convolution of different parameters: expanding velocity of the shell, H I column density along the

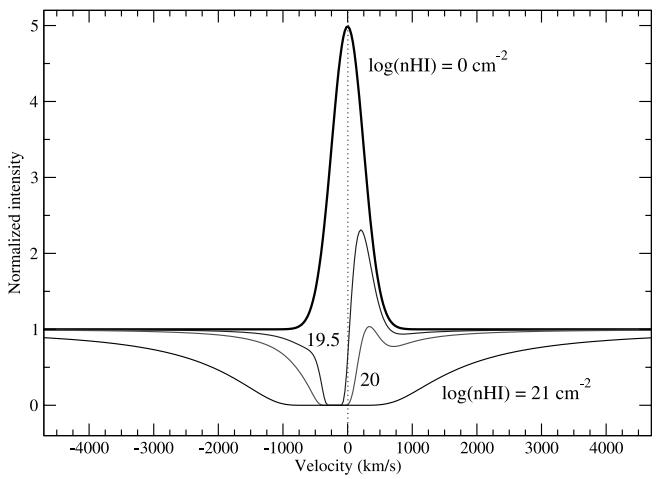

FIG. 15.—Expected Lyα profiles. We have assumed an intrinsic Lyα emission line originating in the central H II region, at systemic velocity ($V = 0$ km s^{-1}). The plot shows the intrinsic emission profile (*thick line*; $\log n$ (H I) = 0 cm^{-2}) and the resulting profiles assuming a slab of neutral hydrogen moving at $v_{\rm exp} = -200$ km s^{-1}, with column densities $\log n$ (H I) = 19.5, 20 and 21 cm^{-2}. [*See the electronic edition of the Journal for a color version of this figure*.]

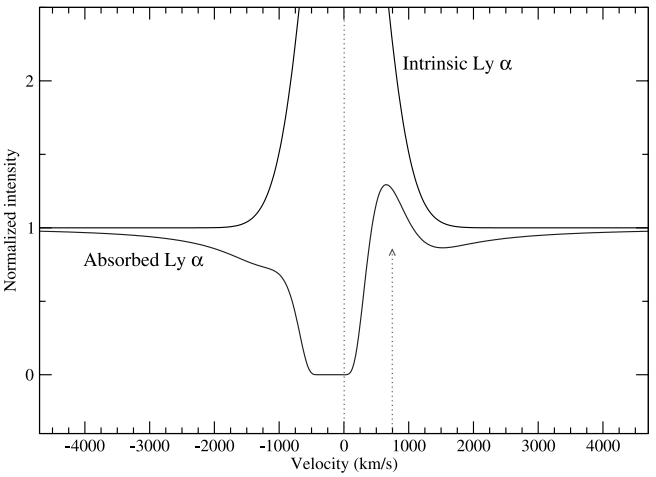

FIG. 16.—Detail of a resulting Lyα profile showing that under certain circumstances the centroid of the observed Lyα emission line can appear redshifted by several hundred km s^{-1}. This redshift, nevertheless, is artificially originated by the absorption of the blue part of the profile, and should not be considered as a tracer of ionized gas outflows. Moreover, it is important to note that the width of the resulting line is much smaller than that of the intrinsic emission line. This example has been computed for $\log n$ (H I) = 20.3 cm^{-2} and $v_{\rm exp} = -300$ km s^{-1}. [*See the electronic edition of the Journal for a color version of this figure.*]

line of sight, intrinsic intensity and width of the central Lyα emission line, etc., so that we expect to detect the different cases presented in Figure 15 almost randomly.

Note that P Cygni Lyα emission profiles show a peak that appears redshifted with respect to the intrinsic line by up to several hundred km s^{-1}. This is shown as an example in Figure 16. The broader the intrinsic Lyα emission line, the redder the peak can appear after partial absorption by an expanding shell. Clearly, the effect of resonant scattering within a dense, expanding neutral shell leading to a redshifted Lyα emission peak should not be taken as evidence for the presence of outflowing, receding ionized gas.

In the presence of a neutral expanding shell we expect to detect interstellar absorption lines associated to the neutral or weakly ionized gas. These will appear blueshifted with respect to the systemic velocity by $-v_{\rm exp}$, as indeed found by Kunth et al. (1998).

If the expanding shell remains symmetric, the internal surface of the receding section of the shell will also affect the observed Lyα profile: a fraction of the ionizing photons can ionize this internal surface of the shell. The photons produced by the approaching section of the shell would be immediately scattered by the neutral gas. Since both the ionized and neutral layers are expected to expand at the same velocity, the absorption would be very efficient, and no photon can escape. On the other hand, photons that originate at the receding section of the shell would be emitted with a redshift corresponding to $+v_{\rm exp}$ and would be able to travel freely through the approaching neutral layers of the expanding shell.

Moreover, a fraction of the photons scattered by the neutral layers on the receding shell will end up being reemitted on the direction of the line of sight, also with a redshift of $+v_{\rm exp}$, and will be able to go through the neutral layers of the approaching shell. As a result, we expect to detect an additional Lyα emission component peaking at $+v_{\rm exp}$. This component should be broader than the intrinsic Lyα line, since the resonant scattering affects photons over a rather wide range of energies. Nevertheless, we expect this component to be rather weak (at a level of few percent of the intrinsic Lyα line), producing just a broadening at the red wing of the resulting Lyα emission profile since most of the photons affected by scattering would be destroyed by dust. This effect is shown in Figure 17, where we have plotted the expected resulting profile, assuming a component that originated at the receding shell (both by photoionization and backscattering) amounting to 10% of the intrinsic Lyα emission line.

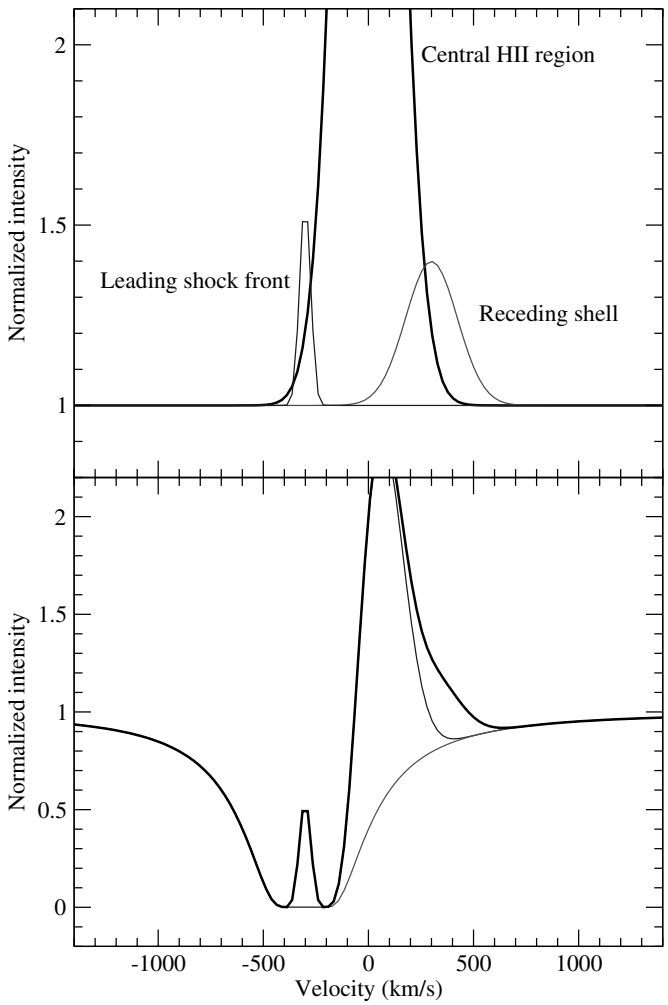

FIG. 17.—Effect on the resulting profile of the additional Lyα emission components. The first contribution originates at the inner part of the receding shell by photoionization and/or backscattering of Lyα photons produced in the central H II region. The example has been computed for $\log n$ (H I) = 19.5 cm^{-2} and $v_{\rm exp} = 300$ km s^{-1}. The intensity of this contribution has been assumed as 10% the intensity of the main Lyα component originated in the H II region, as found by Legrand et al. (1997) for Haro 2. This component should appear redshifted at the velocity of the shell, in this case $v_{\rm exp} = +300$ km s^{-1}, and enhances the base of the red wing. The second contribution to Lyα originates at the ionized region in front of the neutral expanding shell, appearing thus at the velocity of the approaching shell, $v_{\rm exp} = -300$ km s^{-1}. This component is not affected by neutral gas scattering and should appear on top of the damped absorption profile. In the top panel we show the three contributions to Lyα. The thick line is the emission line produced in the central H II region. The lower panel shows with thick line the resulting profile. The thin lines show the assumed absorption profile and the convolved profile of the intrinsic Lyα line alone. The effect of these two additional components on the total resulting profile is evident. [*See the electronic edition of the Journal for a color version of this figure.*]

Ahn et al. (2003) have extended their models (Ahn et al. 2001, 2002) to a spherical, expanding supershell. As discussed in § 3.1, these models do not consider the effects of dust absorption, and allow for multiple backscattering events only on the internal layers of the expanding neutral shell, both on the approaching and on the receding sides. After each backscattering, photons get an additional redshift of $+v_{\rm exp}$, but since no photon destruction is considered, several redshifted emission peaks are produced by multiple backscattering. However, we argue that when absorption by dust is taken into account, multiple peaks anticipated by these authors would disappear. Moreover, the intensity of the single redshifted peak would be much weaker than predicted since most photons affected by scattering are destroyed before being back-emitted. We have not performed a line-transfer model to reproduce this effect. We just qualitatively show that both backscattered photons and the Lyα ones originating at the internal, ionized layers of the expanding shell will produce an additional weak and broad emission component centered at around $+v_{\rm exp}$.

Finally, an ionized region can develop at the external shock front of the shell. The recombining medium immediately behind the shock front would produce an additional Lyα emission line unaffected by resonant scattering. This emission line, observed at a blueshift corresponding to the expansion velocity of the shell, $-v_{\rm exp}$, if present, would fill partially the damped absorption profile. Its redshifted counterpart, on the other hand, will be scattered and fully absorbed within the large column density of neutral matter in the receding part of the shell.

The above discussion aims to confront the reader with the view that there are many parameters related to the structure of the H II region that affect the resulting Lyα profile. In particular, the velocity and density structure of the neutral gas along the line of sight seems to be a dominant factor for the visibility of the line.

4. Lyα EMISSION IN STARBURST GALAXIES: AN EVOLUTIONARY VIEW

In realistic cases, bubbles and superbubbles generated around an H II region will evolve with time, in parallel with the evolution of the massive stars themselves. As a result, the physical conditions that the Lyα photons experience when escaping from the H II region will differ drastically. Therefore, the expected Lyα profiles will be strongly dependent on the geometry and evolutionary state of the starburst.

We show in Figure 18 the predicted evolution of the expanding shells generated by an H II region as they interact with the disk and the halo of the host galaxy. The figure makes use of the results from the numerical calculations presented in Tenorio-Tagle et al. (1999) and illustrates in a simplified way the different elements that determine the properties of the Lyα emission profile. We have identified six basic steps, as follows:

1. Initially, when a star-forming episode starts, a central H II region begins to develop. At this phase, if the neutral gas surrounding the starburst region has H I column densities above 10^{14}–10^{15} cm^{-2}, an absorption line centered at the systemic velocity of the galaxy will be visible, independently of the viewing angle. If the total H I column density along the line of sight is higher than around 10^{18} cm^{-2}, a damped Lyα absorption profile will be detectable. It is important to stress that the Balmer lines will be strongest during this early phase, because of the high-ionizing flux produced by the most massive stars.

2. The situation changes drastically and becomes a strong function of viewing angle once the mechanical energy released by the starburst is able to drive a shell of swept-up matter to exceed the dimensions of the central disk. Then, upon the acceleration that this shell experiences as it enters the low-density halo, it becomes Rayleigh-Taylor unstable and fragments. This event allows the hot gas (composed basically by matter recently processed by the starburst) to stream with its sound speed between fragments and follow the shock, which now begins to form a new shell of swept-up halo matter. Another consequence of blowout is that the ionizing photons from the recent starburst are now able to penetrate into the low-density halo and manage to produce an extended conical H II region that reaches the outskirts of the galaxy. Given the low densities in the halo, it is likely that this matter will remain ionized for a time that well exceeds the duration of the starburst activity. This also implies that some UV photons are at this stage able to stream freely into the intergalactic medium. The predicted expansion speed of this second shell formed in the halo would be around several hundred km s^{-1}.

An observer looking then at the starburst through the conical H II region will be able to detect the strong Lyα emission line produced by the central H II region, centered at the systemic velocity of the galaxy. On the other hand, an observer looking outside the conical H II region will still detect a broad absorption profile at any evolutionary state.

3. Sooner or later, recombination will begin to be frequent enough in the expanding shell. This will cause a strong depletion of the ionizing radiation, which formerly was able to escape the galaxy after crossing the extended conical H II region. Recombination in the expanding shell will produce an additional Lyα component, which the observer will detect as blueshifted according to the expansion velocity of the shell, $-v_{\rm exp}$. Clearly, if the shell were symmetrical and one could see the emission coming from the whole of it, a top-hat line profile would have to be added to the central H II region Lyα emission line. If only a fraction of the shell is observed, we would expect to see two additional emission peaks centered at $\pm v_{\rm exp}$.

4. There are three effects that eventually lead to the trapping of the ionization front within the expanding shell.

a) The first is the increasingly larger amount of matter swept into the expanding shell as this ploughs into the halo.

b) The growth of the shell dimensions also implies fewer UV photons impinging, per unit area and per unit time, on the inner edge of the shell.

c) Finally, in the case of a nearly instantaneous starburst, the production of UV photons starts to decrease drastically (as t^{-5}) after the first 3.5 Myr of evolution.

The trapping of the ionization front will yield the formation of a neutral layer at the external side of the expanding shell. All these effects lead then to an increasingly larger saturated absorption, as the external neutral layer will resonantly scatter the Lyα photons. As discussed above, this absorption will be blueshifted with respect to the Lyα photons emitted by the central H II region by $-v_{\rm exp}$, leading to the formation of a P Cygni profile with a fraction of the intrinsic Lyα emission being absorbed.

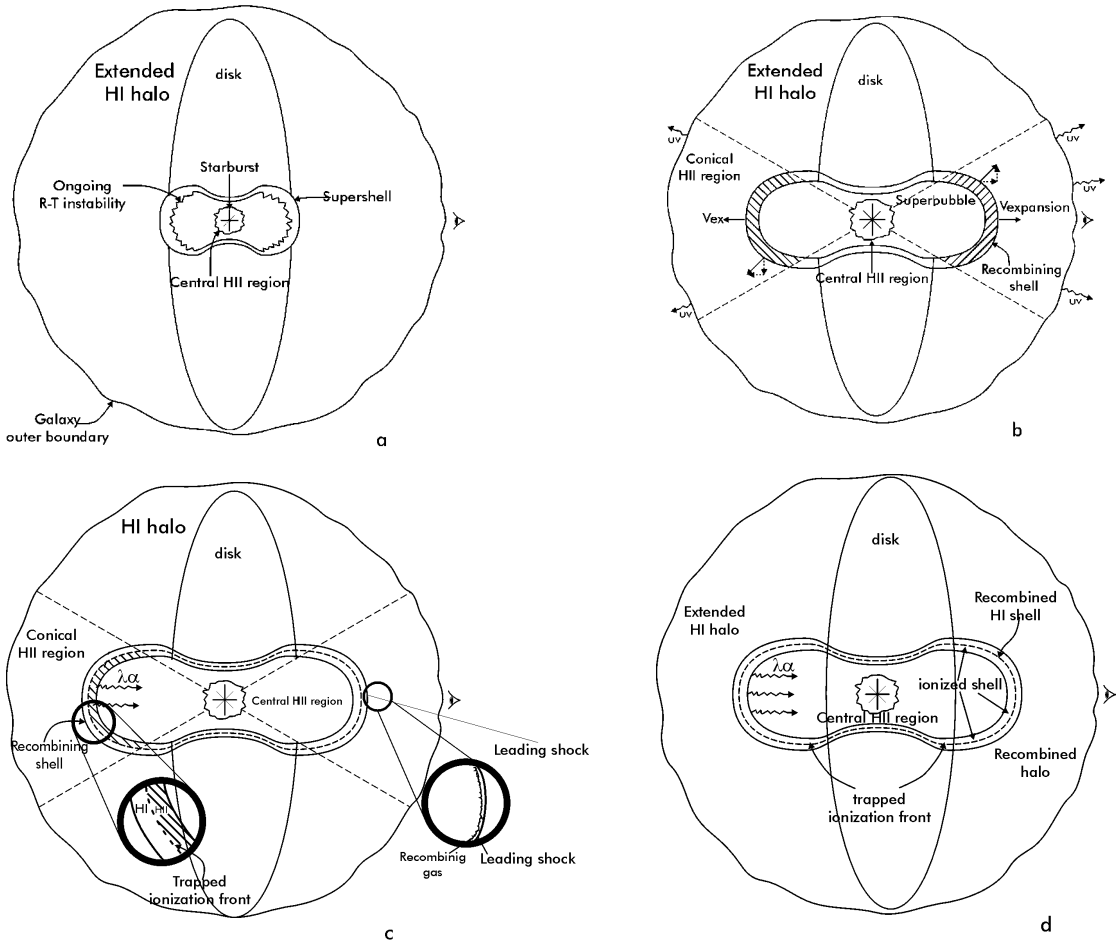

FIG. 18.—Basic model (see Tenorio-Tagle et al. [1999] for further details): evolution of the expanding shell generated by an H II region and implications for the visibility of the Lyα emission line. (*a*) A massive starburst generates a central H II region. The surrounding halo of neutral gas absorbs all photons with energy close to Lyα ones, producing a damped absorption profile. (*b*) At the beginning of the star-formation episode, the number of ionizing photons emitted by the central cluster of massive stars is very large, so that a fraction of them can escape the H II region and produce the ionization of the surrounding halo of the host galaxy. An observer looking straight through the ionization cone will detect a very strong Lyα line centered at the rest velocity of the host galaxy. On the other hand, an observer looking at a higher angle will still see a damped absorption profile produced by the neutral gas on the galaxy disk. (*c* and *d*) The action of stellar winds and supernovae explosions generates an expanding shell that eventually will be able to undergo recombinations and emits also Lyα photons. Furthermore, this large-scale expanding shell, driven by the mechanical energy released by the massive central starburst, is eventually able to trap the ionization front produced by the UV photons that escape the central H II region. This leads to the formation of two zones within the shell, expanding at the same speed. The inner zone is fully ionized and emits in Lyα,while the outer zone is neutral and capable of scattering and absorbing this radiation. The neutral gas in the approaching side of the shell leads to the formation of a Lyα P Cygni line profile, as discussed in the text. In addition, Lyα photons produced by the central H II region and backscattered by the neutral layers of the receding shell will contribute with a low-intensity, broad component redshifted by $v_{\rm exp}$.

In addition, the profile will be contributed to by the Lyα radiation arising from the receding section of the shell, both by recombination on the ionized layer and by backscattering of the central Lyα photons by the neutral layer. Since this contribution will be redshifted by $2 \times v_{\rm exp}$ with respect to the absorbing layer, it will be essentially free from resonant scattering and will be able to escape the region almost unaffected.

Under such circumstances, the resulting Lyα emission line will be strongly depleted, showing a very asymmetric profile with a sharp blue edge and a line centroid shifted toward the red at a wavelength different from the rest velocity of the host galaxy. The red wing of this profile will, furthermore, be broadened by the contribution from the receding shell.

5. Under some conditions (for specific values of the shock velocity V_s and halo density $n_{\rm halo}$), the leading shock front may become radiative. An additional Lyα component would thus arise as the shocked gas undergoes recombination. This should happen after a cooling time [$t_\Lambda = 1.5kT/(4n_{\rm halo}\Lambda)$; where

$$T = 1.4 \times 10^7 (V_S/1000 \text{ km s}^{-1})^2 ,$$

Λ is the cooling rate, and k the Boltzmann constant]. Thus a combination of shock speed and density of the background halo may lead to a t_Λ smaller than the dynamical time and at that moment Lyα emission will be produced as the shocked gas recombines. This additional Lyα emission component would appear blueshifted at $-v_{\rm exp}$ and would not be absorbed being ahead of the H I layers.

6. At a later phase, the shell will be completely recombined and have already substantially slowed down its expansion. Lyα will show a broad absorption with only a small blueshift. The recombination lines from the H II region will be very weak.

The scenario here presented assumes a non–steady state of the star formation process. It implies, therefore, either a

(nearly) instantaneous starburst or the first phases of a star formation episode extended in time. In the case of a continuous star formation regime, a steady state where the birth and death of massive stars balances, so that the ionizing flux remains basically constant, is achieved only after the first 15 Myr of evolution (Cerviño & Mas-Hesse 1994). If the process is active for much longer periods of time, the shell will finally blow out in the intergalactic medium, and pure emission or absorption, depending on the orientation, rather than Lyα emission lines with a P Cygni profile would be expected.

5. GENERAL DISCUSSION

Figure 19 shows three GHRS low-resolution examples corresponding to typical cases as described above. T1214−277 shows a prominent and symmetric Lyα emission line. The large equivalent width of the line ($\sim$90 Å) points to a very young starburst. We postulate that this object would correspond to steps 2 and 3 above. In IRAS 0833+6517 the ionization front has already been trapped, so that a neutral layer has already developed, giving rise to a blueshifted absorption and a corresponding P Cygni profile (step 4). Moreover, an additional blueshifted emission component can be easily identified in higher resolution images (see Fig. 9), as proposed in step 5. Finally, SBS 0335−052 shows a very broad, damped Lyα absorption line. This could hint to a very young object (step 1) or to a geometrical effect, if we were observing from outside the ionization cone and through dense layers of static neutral gas.

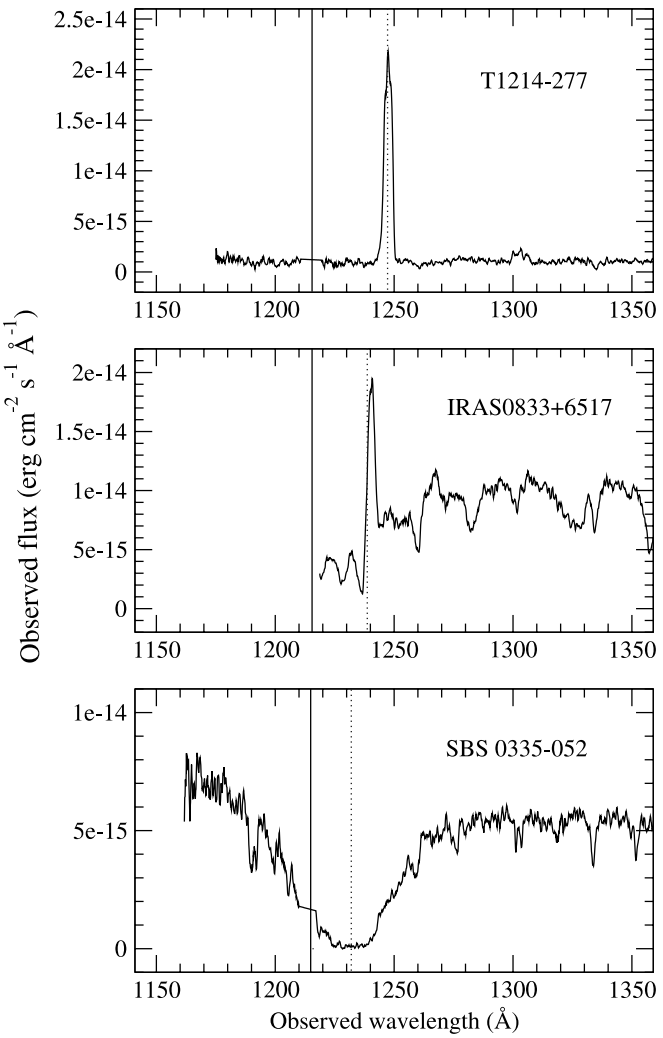

FIG. 19.—Observed Lyα profiles illustrating the different cases discussed in the text: pure emission, with only weak absorption possibly produced by extinction (*top*), P Cygni profile produced by a partially neutral expanding shell (*middle*), and completely damped absorption produced by essentially static neutral gas (*bottom*). [*See the electronic edition of the Journal for a color version of this figure.*]

In this section we discuss in more detail the observed properties of the different objects considered and how they fit within the proposed scenario.

SBS 0335−052.—SBS 0335−052 is a metal-deficient blue compact galaxy that is hosting a very strong star-forming episode. Its morphology and properties were described by Thuan, Izotov, & Lipovetsky (1997). They identified six super–star clusters containing an equivalent of $\sim$4500 ionizing O7 stars. This galaxy is embedded in a large H I cloud with a mass of $\sim 10^9\ M_\odot$. The H I column density along the GHRS aperture measured by these authors is very large, $N(\mathrm{H\ I}) = 7.0 \times 10^{21}$ cm^{-2}. The observational properties of SBS 0335−052 would be consistent with step 1: a very young starburst starting to ionize the surrounding medium while a significant amount of H I gas remains in front of the massive stars and is still static with respect to the central H II region. As a result, while a strong emission-line spectrum is seen in the optical, the spectral region around Lyα is completely absorbed, showing a damped absorption profile, similar to the ones computed in Figure 14.

Kunth et al. (1998) identified the O I and Si II absorption lines attributed to the neutral gas at the same redshift than the central H II region. Thuan & Izotov (1997) postulated the presence of two additional O I and Si II absorption systems blueshifted by 500 and 1500 km s^{-1}, which might indicate that some layers of H I could be starting to be accelerated by the release of mechanical energy from the starburst, as expected in step 1 (see Fig. 18*a*).

Figure 20 shows the presence of a marginal excess emission in the wings of the Voigt profile, suggesting an intrinsically very strong Lyα emission line. We have fitted the intrinsic Lyα profile that would produce such an excess, after convolution with the absorption expected by the large amount of neutral gas, deriving a very strong emission with $W(\mathrm{Ly}\alpha) = 120$ Å, consistent with a very young and powerful starburst.

I Zw 18.—The GHRS high-resolution spectrum of I Zw 18 was first discussed by Kunth et al. (1994) and was reanalyzed by Kunth et al. (1998). It resembles very much the spectrum of SBS 0335−052, with a broad, damped Lyα absorption profile corresponding to an H I column density $N(\mathrm{H\ I}) \sim 3.0 \times 10^{21}$ cm^{-2}. I Zw 18 is also a metal-deficient blue compact galaxy surrounded by a dense cloud of neutral hydrogen. Kunth et al. (1998) showed that the O I and Si II interstellar absorption lines were at the same redshift as the central H II region, indicating that the neutral gas is unperturbed and mostly static with respect to the starburst region.

As discussed above, no Lyα emission is detected along the STIS slit, suggesting that a static neutral gas cloud completely covers the ionized region with a large column density along the line of sight. This case seems in principle to be similar to SBS 0335−052. Nevertheless, while the starburst in this latter galaxy seems to be very young, there are hints for a continued massive star formation activity in I Zw 18 over

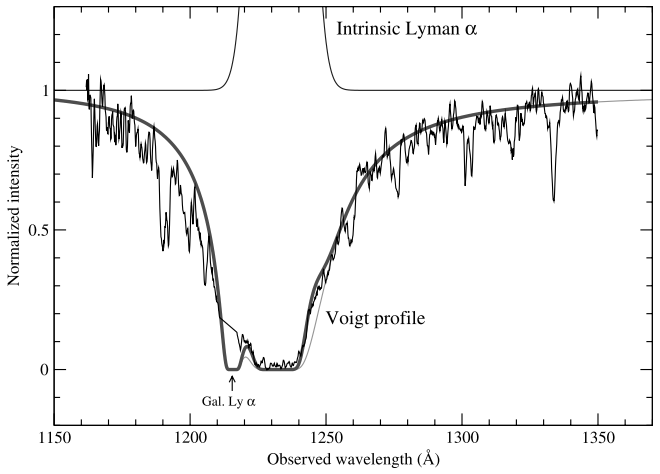

FIG. 20.—Detail of the damped Lyα absorption profile in SBS 0335−052. The thin line corresponds to the fitted Voigt absorption profile, including also the effect of the Galactic absorption. The thick line shows the convolution of the intrinsic emission line and the total absorption profile. It can be seen that the observed profile shows an excess with respect to the theoretical Voigt profile, detectable on both the red and the blue wings. We interpret this excess as the wings of the intrinsic Lyα emission line generated in the H II region, which become partially visible since the absorption at these wavelengths is not total, as evident from the Voigt profile. The H II region Lyα emission required to reproduce the observations would have an equivalent width around 120 Å, as expected for a very young starburst. [*See the electronic edition of the Journal for a color version of this figure*.]

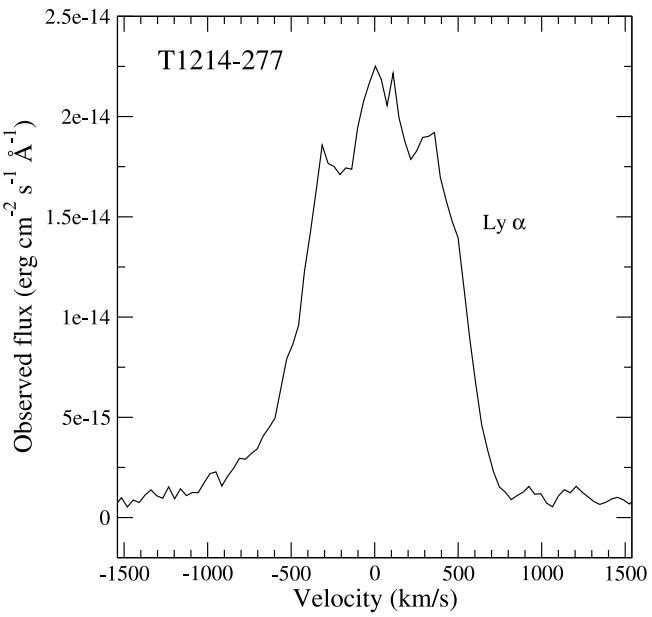

FIG. 21.—Detail of the T1214−277 Lyα emission profile in velocity scale. The two peaks identified at $\sim\pm300$ km s^{-1} from the central line peak could be attributed to the secondary emission from the approaching and receding parts of the young shell, according to steps 2 and 3 in the text. [*See the electronic edition of the Journal for a color version of this figure*.]

the last 10–15 Myr (Mas-Hesse & Kunth 1999), although at a rather weak rate. Moreover, large supershells and ionized filaments have been identified in this galaxy by Martin (1996). The observer might be looking in this case through the large amounts of static neutral gas expected outside the conical H II region, which could be located along the supershells detected in the optical.

T1214−277.—The low-resolution GHRS spectrum of T1214−277 has been described in detail by Thuan & Izotov (1997). This very low-metallicity galaxy ($\sim Z_{\odot}/23$) hosts a very young and massive starburst. As these authors quote, this galaxy has a large Lyα equivalent width ($\sim$70 Å). Campbell, Terlevich, & Melnick (1986) measured also a very large Hβ equivalent width [$W(\mathrm{H}\beta) \sim 320$ Å within a $2'' \times 4''$ aperture]. No intrinsic extinction was measured by these authors from the Balmer lines ratios (but note that the Galactic extinction alone, with $E(B-V) = 0.06$, destroys around 45% of photons in the Lyα region). The high equivalent widths and the absence of Wolf-Rayet features (Pagel et al. 1992) indicate that the starburst in T1214−277 has to be younger than 3 Myr, at which time the first massive stars enter the Wolf-Rayet phase at low metallicities (Mas-Hesse & Kunth 1999).

These observational results indicate that T1214−277 could be at the end of step 2, as explained above: a conical H II region would have already developed, so that an observer looking through it could detect the strong Lyα emission produced by the central H II region without significant distortion.

In Figure 21 we show a detail of the Lyα emission profile in velocity scale. The profile is broadened, with two symmetric secondary peaks located at $\sim\pm300$ km s^{-1} from the central emission peak. We postulate that the starburst in this galaxy may be indeed already entering step 3, so that recombination within the expanding shell produces the additional Lyα components. Since only a fraction of the shell is seen through the GHRS aperture, the observer detects only two additional peaks, centered at $\pm v_{\mathrm{exp}}$. The velocity derived for the shell (300 km s^{-1}) is within the expected range (a few hundred km s^{-1}) and is similar to velocities measured in the other starburst galaxies with P Cygni profiles.

Haro 2.—Haro 2 is a well-studied, rather metal-rich blue compact galaxy. As described by Lequeux et al. (1995) and Kunth et al. (1998), Haro 2 shows a prominent Lyα emission line, with a clear P Cygni profile. The metallic O I and Si II interstellar absorption lines are detected at around -200 km s^{-1} with respect to the central H II region, without any significant absorption feature detected at the redshift of the H II region. Haro 2 would be the prototype of our step 4, with a shell of neutral gas expanding at around 200 km s^{-1} with respect to the central H II region, ploughing into a low-density, ionized halo without a screen of static neutral gas.

From the STIS long-slit spectral images (Fig. 1) we can identify all the features expected in step 4:

1. The emission decreases rapidly blueward of the velocity at which the emission peak originated from the central H II region. The flux goes to zero at basically the same velocity all along the slit. As discussed in § 2, this is consistent with an expanding shell of neutral gas, which has to be much more extended than the 8″ over which the absorption is detected in order to behave as a plane-parallel slab. From the analysis of Hα long-slit spectroscopy Legrand et al. (1997) found evidence for the presence of an ionized expanding shell over a region around 25″ in diameter (nearly 2.4 kpc). The lateral edges of the shell appeared at the same systemic velocity as the central H II region, decoupled, as expected, from the disk rotation. The Hα line is also clearly broadened at the

edges, in good agreement with what would be expected from an expanding shell.

As explained above, step 4 foresees that as the starburst evolves, the trapping of the ionization front will yield the formation of a neutral layer at the external side of the expanding shell, with no static neutral gas inside the shell. This would produce the kind of profile we detect on the central region of Haro 2 (see Figs. 3 and 15).

2. At the same time, recombination on the internal layers of the shell produces additional emission components at $\pm v_{\rm exp}$, in this case at ± 200 km s^{-1}. While the blueshifted Lyα emission component produced in the internal layers will be destroyed by resonant scattering on the external neutral layers (both expanding at the same velocity), this blueshifted emission should be detectable in Hα. Legrand et al. (1997) indeed concluded that the Hα emission profile (when looking straight into the starburst region) showed evidence of two additional weak components at ± 200 km s^{-1}.

These results indicate that a section of the shell receding at the same velocity should also be present. The internal part of the receding shell would produce Lyα photons, since it generates Hα ones. And the neutral layers of the receding shell would backscatter in addition some Lyα photons produced at the central H II region. Since the receding neutral gas lies at $-v_{\rm exp}$ with respect to the central H II gas, it scatters the blue wing of the intrinsic Lyα emission profile. A key point is that this receding shell lies at $+2 \times v_{\rm exp}$ with respect to the approaching shell, so that the Lyα photons emitted or backscattered there traverse unaffected the approaching neutral layers and reach the observer redshifted by $+v_{\rm exp}$. As a result, we expect an extended broad and weak component of Lyα photons centered at around $+200$ km s^{-1} in the case of Haro 2 (see the example in Fig. 17).

This is exactly what we detect in our spectral images (Fig. 1). A weak extended emission is detected at both sides of the central H II region on the slit, but especially to the upper side. It results from the Lyα photons originating from or backscattered by the receding shell. We show in Fig. 4 the profiles of this emission at several arcseconds from the central H II region. The profiles show the following:

a) In both parts of the slit, southwest and northeast of the central H II region, the blue edge of the emission profile lies at the same velocity: the approaching neutral shell is destroying all photons blueshifted with respect to the velocity of the central H II region.

b) Broad extensions up to around $+500$ km s^{-1}. Profiles are more symmetric than the central Lyα emission line, and their peaks are clearly redward of the Lyα peak. Both profiles show quite extended red wings at basically the same velocity. These wings originate by recombination and backscattering in the ionized and neutral layers of the receding shell, respectively. Since the scattering process affects photons within a high range of velocities, as shown in Figure 4, the backscattered component should cover basically the same velocity range measured on the absorption profile. We consider indeed that the good agreement between the terminal velocity of the P Cygni profile (around -500 km s^{-1}) and the terminal velocity of the extended Lyα emission profile (around $+500$ km s^{-1}) supports our interpretation.

IRAS 0833+6517.—As discussed in § 2, Lyα emission in IRAS 0833+6517 has a more complex structure than in Haro 2 (see Fig. 7). In addition, a secondary Lyα emission is conspicuous on top of the damped absorption. Nevertheless, the overall properties of the Lyα emission are very similar in both galaxies:

1. The flux vanishes blueward of the same wavelength along the slit (hence the same velocity) whenever Lyα emission is detected (10″, 4.1 kpc). The extension of the neutral gas shell has to be very large in this galaxy, reaching a diameter close to 10 kpc.

2. South and north of the central region where Lyα is in emission, we again detect an extended broad and weak component redshifted with respect to the central H II region by around 300 km s^{-1}. The terminal velocity of the Lyα profile all along the slit is at around $+700$ km s^{-1}. As in Haro 2, we associate this component with the emission originated at the receding shell, both by the ionized inner layers and by backscatter in the neutral external layers.

We therefore argue that the superbubble phase in IRAS 0833+6517 corresponds to step 4 in our model. The presence of an additional emission component on top of the absorption profile, blueshifted by around -300 km s^{-1} with respect to the central H II region, supports our interpretation that an expanding shell is moving toward the observer at this velocity. As explained in step 5, the leading shock in this galaxy should have already become radiative, undergoing recombination and originating the secondary Lyα emission line that we detect at the velocity of the shell. The fact that this secondary emission does not appear to be affected by neutral gas scattering indicates that the H I column density in front of the expanding shell (either static or also expanding) has to be rather small, as expected in our model. The smaller spatial extension of this secondary emission indicates that only a fraction of the whole surface of the leading shock is undergoing recombination. Conditions given in step 5 strongly depend on the density of the halo, which is most likely not uniform, explaining the patchiness of this emission.

We have overplotted in Figure 22 our high-resolution STIS spectrum of IRAS 0833+6517 over the lower resolution GHRS one presented by González Delgado et al. (1998). This comparison exemplifies how the analysis of P Cygni profiles at low resolution may yield misleading

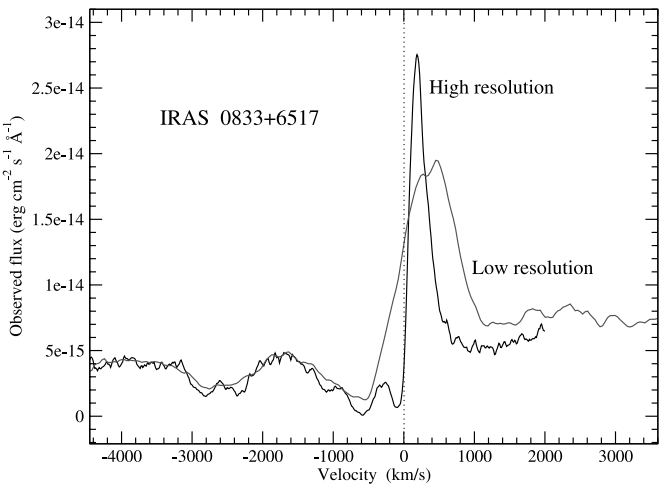

FIG. 22.—Detail of the IRAS 0833+6517 Lyα profile observed at two different resolutions. Note that low-resolution spectroscopy can hide the presence of a blueshifted damped Lyα absorption profile. [*See the electronic edition of the Journal for a color version of this figure.*]

results. The asymmetry of the intrinsic profile translates into an artificial redshift of the emission-line peak when observed at low resolution (in addition to the effect discussed in § 3, Fig. 16). This effect might be especially severe when analyzing galaxies at high redshift with medium- or low-resolution spectra. Furthermore, the lower resolution does not allow us to identify the damped, black absorption plateau (which in this case is partially filled by the secondary emission peak), preventing an accurate derivation of the intervening H I column density.

We want to remark that our model provides a simplified scenario for the formation of Lyα P Cygni profiles in starburst regions. The actual geometry and kinematical structure of some objects, such as IRAS 0833+6517, might be significantly more complicated, although the overall view should still be valid. Let us highlight some observational properties that may be relevant:

1. Kunth et al. (1998) were not able to detect the interstellar O I λ1302.2 and Si II λ1304.4 lines in their high-resolution GHRS spectrum. The analysis of the lower resolution data from González Delgado et al. (1998) shows that both lines are blended within a very broad absorption profile, which in fact was extended over most of the Kunth et al. (1998) GHRS wavelength range. González Delgado et al. (1998) report also very broad profiles on other interstellar lines, with FWHM of up to around 1000 km s^{-1}. They interpret these broad absorption profiles as evidence of large-scale motions of the interstellar gas around the starburst region.

2. The Si III λ1206 absorption line detected blueward of 1230 Å is split into two components (see Figs. 7 and 9). While the weaker component is centered at the redshift of the central H II region, the stronger one appears blueshifted by around -470 km s^{-1}, which is higher than the expansion velocity attributed to the shell. González Delgado et al. (1998) also found from lower resolution GHRS spectra that the interstellar Si II λ1260 and C II λ1335 were blueshifted by 450–520 km s^{-1} with respect to the central H II region. We want to stress that no Lyα emission at around -500 km s^{-1} can be detected. Therefore, the high-velocity gas has to be contained within the expanding shell.

We conclude that while the bulk of the neutral gas shell seems to be expanding at around 300 km s^{-1}, some gas might be moving within the shell in a rather chaotic way at significantly higher velocities.

Other galaxies.—The model we have proposed could also explain the observational properties of the Lyα line in other starbursts studied up to now. II Zw 70 and Mrk 36, discussed by Kunth et al. (1998), and Tol 65, presented by Thuan & Izotov (1997), would be similar to I Zw 18 and SBS 0335−052: they show a damped broad absorption profile, and their interstellar absorption lines appear at the redshift of the central H II region. The H I gas is therefore static along the line of sight with respect to the H II region, either because their starburst episodes have not been able to accelerate the gas (being very young or weakly energetic compared with the amount of neutral gas surrounding them) or because we are observing them through the densest part of the H I disk. In this latter case, Lyα emission could possibly leak from other regions (for instance if an ionizing cone is allowing the photons to escape) and it might be scattered to our line of sight.

We are presently performing a survey with the *HST* Advanced Camera for Surveys looking for regions in this kind of galaxies where Lyα photons could be leaking. Preliminary results appear in Kunth et al. (2003).

Other galaxies studied by Kunth et al. (1998), that show P Cygni Lyα absorption and blueshifted interstellar lines, such as ESO 400−G043 and ESO 350−IG038, would also be in the state described by our step 4, which seems to be the most frequent one among the galaxies showing Lyα emission.

We want finally to stress that the expanding layer causing the typical P Cygni Lyα line profile in starburst galaxies is extended and can span several kiloparsecs across a galaxy. As discussed above, in some objects this can be traced across several hundreds of parsecs away from the main burst of recent star formation. In the case of IRAS 0833 this spans more than 10 kpc across the galaxy. Our observations thus prove that this is not a well-localized phenomenon but rather a large-scale one affecting the whole central region of these galaxies. Nevertheless, to explain the properties of this emission (lack of structure and clumpiness, velocity dispersion, and intensity), the low-density medium or halo of the host galaxy, into which the shell propagates, has to be very extended so as to allow for the existence of a continuous shell with similar properties (column density, velocity, etc.) over dimensions $\geq$1 kpc. If this were not the case and the expansion had reached the galaxy edge, upon blowout the shell would have become Rayleigh-Taylor unstable and would have rapidly broken while destroying the absorbing layer. Thus, although the Lyα asymmetric line profiles are indicative of strong outflows, these do not certify that supergalactic winds, venting the metals from the newly formed starbursts into the intergalactic medium, have already developed. In fact, if the expanding shell could reach the edge of its host galaxy, becoming Rayleigh-Taylor unstable and fragmenting, the Lyα line profile to be observed would be the almost unattenuated line produced by the central H II region, without any absorption by neutral gas, not the kind of profile generally observed.

6. IMPLICATIONS FOR GALAXIES AT HIGH REDSHIFT

It is expected that all L^* galaxies have undergone a phase of rapid star formation at a certain stage of their evolution. During this phase they should have become very powerful producers of ionizing photons. Very strong emission lines are therefore expected from these objects, and with rather large equivalent widths. For redshifts above $z \sim 3$, the Lyα emission line would be observable in the optical range, making it therefore a priori an optimal tracer of star formation. Nevertheless, the first searches did not detect Lyα emitters. It has been only recently that Lyα emission from galaxies at redshifts above $z \sim 3$ has been detected, but at average luminosities weaker by 2 orders of magnitude than expected (see Rhoads et al. [2000] for a complete set of references concerning Lyα emission at high redshift).

Our analysis of Lyα emission-line properties in nearby starburst galaxies has shown that there are several issues affecting the shape and intensity of the line, so that only in a small fraction of the cases would the full intrinsic emission be detectable. In this section we will extrapolate our results to high-redshift galaxies, aiming to estimate the expected properties of Lyα emission in these objects.

Star-forming episodes detected in galaxies at redshift $z \sim 3$ seem to be significantly stronger than those detected in compact galaxies in the nearby universe (see Shapley et al. 2001, 2003 and references therein). Nevertheless, the properties of the Lyα emission profiles are very similar to those observed in local starbursts. Lyman break galaxies exhibit a broad distribution of Lyα strengths and profile types, ranging from damped absorptions to pure emission, including also P Cygni–like absorption and emission combinations (Shapley et al. 2003). Asymmetric P Cygni profiles have also been detected by Frye, Broadhurst, & Benítez (2002) and Pettini et al. (2000, 2001), among other authors (see also Heckman 2001; Rhoads et al. 2000).

Pettini et al. (2001), observing Lyman break galaxies, found velocity offsets of the interstellar absorption lines with respect to the velocity of the H II region, assumed to be at the systemic velocity of the galaxy. They found blue velocity offsets between approximately -200 and -400 km s^{-1} in three-quarters of the objects, with a median value of -300 km s^{-1}. More recently, Shapley et al. (2003) have obtained a composite spectrum by combining the data of 811 individual Lyman break galaxies. This spectrum reveals that the strong low-ionization interstellar features appear blueshifted with respect to the systemic velocity by an average of -150 ± 60 km s^{-1}. Moreover, the mean velocity of the interstellar Si IV doublet is close to -180 km s^{-1}, indeed very similar to the value measured for low-ionization lines. As discussed above, the presence of blueshifted interstellar lines hints directly to the presence of neutral shells expanding at few hundred km s^{-1}, as concluded by Pettini et al. (2001) and Shapley et al. (2003). On the other hand, the simultaneous detection of Si IV at roughly the same velocities suggests that the internal layers of the expanding shells are probably ionized, as discussed above. This range of velocities is consistent with the predictions for a wind-blown shell, as we have seen. On the other hand, these authors found the Lyα emission lines to be always redshifted with respect to the H II regions. The offsets measured for Lyα in the galaxies showing blueshifted interstellar absorptions span a range between around $+200$ and around $+600$ km s^{-1}. The composite spectrum of Shapley et al. (2003) gives a mean redshift of $+360$ km s^{-1} for the Lyα peak with respect to the systemic velocity. As explained above this is exactly what one expects if the central starbursts were driving a neutral (or partially ionized) expanding shell (see Fig. 16).

Pettini et al. (2000) show a high-resolution, high signal-to-noise ratio spectrum of MS 1512$-$cB58, a galaxy at $z = 2.73$. They found a weak and asymmetric Lyα emission line, redshifted by around $+230$ km s^{-1} with respect to the H II region, on top of a damped absorption with $N(\mathrm{H\ I}) = 7.5 \times 10^{20}$ cm^{-2}, blueshifted by -390 km s^{-1} (in agreement with the interstellar lines). At this rather high H I column density the absorption profile is very broad, allowing only a small fraction of the intrinsic Lyα emission-line photons to escape. A careful analysis of their Figure 4 shows the presence of a broad red wing, extending up to $\sim$800 km s^{-1} (velocity measured with respect to the H II region). We postulate that this red-wing component might be emission that originated at the receding part of the shell, either by recombination or by backscattering of Lyα photons from the central H II region, as discussed above. We expect this component to be broader the higher the H I column density, since backscatter would affect photons at increasingly high velocities. The presence of the broad red wing provides additional support for the existence of a rather symmetrical expanding shell being energized by the central starburst.

Asymmetric Lyα emission profiles have also been detected by Frye et al. (2002) on a sample of eight lensed galaxies at high redshift, $3.7 < z < 5.2$. Interstellar absorption lines have also been detected in some of these galaxies, but unfortunately the redshift of the central H II region is not available. They found an offset between the redshift of the interstellar lines and that of the Lyα emission centroid in the range 300–800 km s^{-1}. If we assume that the interstellar lines are tracing a neutral shell that is expanding at around 200–300 km s^{-1} with respect to the central H II region, the Lyα lines detected would be redshifted by up to around 400–500 km s^{-1} at most, in agreement with the predictions and with other galaxies. Note that Frye et al. (2002) always quote the offset between Lyα and the interstellar lines as the local redshift of the Lyα profile, something that is misleading since the shift with respect to the H II region has to be necessarily smaller. Finally, most of the Lyα profiles plotted by Frye et al. (2002) in their Figure 13 show a weak broadening of their red wing, in agreement with the model discussed in this work.

Another important result obtained by Shapley et al. (2003) from their analysis of Lyman break galaxies is that the Lyα emission strength increases as the kinematic offset between the Lyα emission peak and the low-ionization interstellar absorption lines decreases. In addition, the Lyα equivalent width in emission increases as the interstellar lines become weaker. We interpret these effects as an evidence that the lower the neutral gas column density, the smaller the relative redshift of the Lyα emission peak and, correspondingly, the stronger the emission. This is in very good agreement with our above discussion (see, e.g., Fig 16).

We therefore conclude that the properties of the Lyα emission profiles are very similar in local starbursts and in high-redshift galaxies. Nevertheless, there are some differences between both kinds of objects that have to be taken into account for a correct interpretation of the data:

1. Since the star-forming episodes observed at high redshift are very powerful ones, we expect intrinsically very strong Lyα emission lines, with emission extending over several hundreds km s^{-1} at the base of the line. Even accounting for H I column densities around 10^{20} cm^{-2}, photons at the red wing of the emission profile will be able to escape. Therefore, most of these high-redshift galaxies experiencing strong starbursts should show Lyα emission, albeit reduced by large factors from their intrinsic luminosity. Only galaxies with H I column densities above $\sim 10^{21}$ cm^{-2} will show a damped Lyα absorption.
2. For the same reasons we expect the observed Lyα emission lines to appear redshifted with respect to the systemic velocity of the galaxies by a broad range of velocities, up to several hundred km s^{-1}. This effect should be smaller in local starbursts, since the Lyα emission lines would be intrinsically weaker (and therefore narrower at their base). If no other line is available to measure the redshift, one should bear in mind that the derived value is only an upper limit of the galaxy redshift and that the real one might be indeed smaller by several hundred km s^{-1}.
3. The spectra presented by Frye et al. (2002) show a feature that appears only for galaxies at high redshift: the

Lyα forest, which significantly lowers the average continuum blueward of Lyα. As a result, the blue wing of the absorption produced by the local expanding shell cannot be identified in low-resolution data.

On the other hand, the presence of asymmetric Lyα profiles together, with a discontinuity in the continuum (the average continuum redward of Lyα being stronger than blueward of the line), should allow us to identify Lyα in surveys aiming to estimate redshifts of galaxies at high redshift.

4. Stellar Lyα absorption lines might be important at low resolution, artificially decreasing the observed intensity of the Lyα emission line. At high resolution the stellar profiles can be detected and taken into account when measuring the line flux, but at low resolution both profiles might be blended and the emission line substantially hidden (see Valls-Gabaud 1993).

It is clear from the above discussion that using the Lyα emission line as a tracer of star formation episodes might lead to severe errors. We remark that both the measured line intensity, and thus the star formation rate derived from it, as well as its velocity, have to be considered as, respectively, lower and upper limits only. The problem might be especially significant in the case of star formation rates derived from Lyα luminosities, which might be underestimated by more than an order of magnitude.

From the above discussion we see that P Cygni Lyα profiles are predicted only when the superbubble has entered the phase in which the ionization front is trapped by the sector of the shell, which is evolving into the extended halo. It has been noted by Tenorio-Tagle et al. (1999) that P Cygni profiles are seen in galaxies that are on the higher luminosity side of the distribution ($M < -18$) in their sample. Similarly, at high redshift the Lyman break galaxies exhibit similar profiles, as discussed above. Hence, despite the much larger strength of the starbursts they are hosting, as compared to local ones, the H I gas is still present between the H II region and the observer. In particular, this implies that in all these cases the ionizing radiation has to be trapped and that a low-density halo is surrounding these objects; as discussed above, without this halo the shell would have been disrupted and no P Cygni profile would be produced.

It is interesting to relate this result to the constraints on the Lyman continuum (hereafter LyC) radiation from galaxies. Most of the previous observations of galaxies below the Lyman break (Leitherer et al. 1995; Hurwitz, Jelinsky, & Dixon 1997), as well as recent measurements obtained from *Far Ultraviolet Spectroscopic Explorer* observations (Deharveng et al. 2001; Heckman et al. 2001), show that the fraction of ionizing stellar photons that escape the interstellar medium of each galaxy is small, if any. Most estimates led to an escape fraction $\leq 5\%$. However, these figures are in contrast with a LyC escape fraction larger than 50% reported by Steidel, Pettini, & Adelberger (2001), obtained from a composite spectrum of galaxies at $\langle z \rangle = 3.4$. Indeed, starburst galaxies at large redshift have a higher UV luminosity than most local starbursts studied so far. This would imply more photons for ionizing the gas and probably an easier escape. However, this difference remains a puzzle since one must reconcile two facts that seem to contradict each other. One is the leaking of the UV LyC, and the other is the presence of P Cygni Lyα profiles. The very presence of these P Cygni Lyα profiles testifies that a substantial amount of H I is present and hence should act as a screening agent against the escape of the LyC. One way out would be to assume that the H I layers are very perturbed and chaotic, so that they do not completely cover the massive stellar clusters. However, the Lyα emission that would escape from regions devoid of neutral gas should be overwhelming, resulting in a symmetric Lyα emission profile. We predict, therefore, that LyC photons would be detected mostly on galaxies showing strong and quite symmetric Lyα emission lines, rather than in objects showing typical P Cygni profiles. As far as we know, no relation has yet been established between the fraction of escaping LyC and the Lyα emission profile in galaxies hosting starbursts at any redshift.

There is a final point we want to remark. As discussed at the end of § 4, the detection of Lyα P Cygni favours short-lived (or nearly instantaneous) bursts rather than steady state, long-lasting star formation processes. After long-lasting star formation episodes, the expanding shell would have finally blown out in the intergalactic medium, and no P Cygni profiles would be expected on the Lyα lines. We would rather expect to detect pure emission or absorption, depending on the orientation of the line of sight with respect to the disk of the galaxy. In the case of short-lived starbursts, the usual concept of star formation rate (amount of gas mass being transformed into stars per unit time) becomes meaningless: in most starbursts, massive star formation has probably already ceased a few megayears ago. It therefore might be misleading to derive the star formation rate density at high redshift from the analysis of galaxies that are forming stars in short bursts. To solve this inconsistency, we propose to parameterize the strength of these star-forming episodes by the total amount of gas transformed into stars, rather than by the rate of star formation, and to reevaluate accordingly the history of star formation in the early universe. This analysis is beyond the scope of this work and will be presented in a forthcoming paper.

7. SUMMARY AND CONCLUSIONS

Our findings have important implications for the study of Lyα profiles in star-forming galaxies in particular and for superbubble evolution and galactic winds in general. We find that the P Cygni profiles are extended, smooth, and span several kiloparsecs covering a region much larger than the starburst and comparable to or larger than the host galaxy itself. This strongly suggests the existence of an expanding supershell generated by the mass and energy loss of the starburst interacting with an extended low-density gaseous halo.

We identify six phases in the predicted evolution of a supershell that correspond to the different types of Lyα profiles observed.

1. *The early phase*.—In a very young starburst the recombination lines will be at their maximum strength and Lyα will show a broad absorption centered at the systemic velocity of the galaxy. SBS 0335 could be in this stage.

2. *The emission phase*.—The supershell breaks, and ionizing radiation escapes into the low-density halo fully ionizing a "biconical" region. Lyα is in emission at the systemic velocity of the galaxy.

3. *Late emission phase*.—Recombination starts to dominate in the expanding shell, producing an additional Lyα

component shifted by the shell expanding velocity. T1214 would be at the end of phase 2, starting already this phase.

4. *Shell recombination phase*.—Recombination dominates this phase, which is characterized by a strong P Cygni–type profile in Lyα. The absorption component is blueshifted by v_{exp}, the expansion velocity of the shell. Lyα emission is strongly depleted, and the centroid of its profile is shifted toward the red. Backscattering and emission from the receding part of the shell may give raise to an extended red wing in the observed Lyα profile.

5. *Blueshifted component phase*.—If the leading shock becomes radiative, an additional unabsorbed and blueshifted component of Lyα may be produced.

6. *Late phase*.—The shell is almost completely recombined and has substantially slowed down its expansion. Lyα will show a broad absorption with only a small blueshift. The recombination lines from the H II region will be very weak.

These six phases and the associated four different profiles are able to describe, both qualitatively and quantitatively, the variety of observed profiles in both the nearby *HST* sample and high-redshift star-forming galaxies. Given that the probability of occurrence of a given profile depends mainly on the age of the starburst (and also on the orientation), the observed fraction of systems in the different phases will provide important information to critically test the predictions of this scenario.

Our results stress the importance of the density and kinematical structure of the neutral gas surrounding an H II region on the detectability of the Lyα emission. The observed properties of the Lyα emission line will be a convolution of several effects. While the amount of dust alone determines only the absolute intensity of the emission line, but without affecting its equivalent width, the kinematical configuration of the neutral gas is the driving factor for its final visibility and its profile shape—from broad absorption to pure emission. The fact that several independent effects play such a significant role on the properties of the observed Lyα emission lines explains the lack of correlations established in the past between the Lyα emission strength and other properties of different starburst galaxies. The use of Lyα as a tracer of star formation rate, and even as a redshift indicator for galaxies at high-z, should be done with care, always being aware of its limitations.

J. M. M. H. has been partially supported by Spanish grant AYA2001-3939-C03-02. E. T. has been partially supported by the Mexican Research Council (CONACYT) grant 32186-E. She also gratefully acknowledges the hospitality of the IoA in Cambridge. This work was supported by grant GO-08302.01-97 from the Space Telescope Science Institute, which is operated by the Association of Universities for Research in Astronomy, Inc., under NASA contract NAS5-26555.

REFERENCES

Ahn, S., Lee, H., & Lee, H. M. 2001, ApJ, 554, 604
———. 2002, ApJ, 567, 922
———. 2003, MNRAS, 340, 863
Bithell, M. 1991, MNRAS, 253, 320
Calzetti, D., & Kinney, A. L. 1992, ApJ, 399, L39
Campbell, A., Terlevich, R. J., & Melnick, J. 1986, MNRAS, 223, 811
Cerviño, M., & Mas-Hesse, J. M. 1994, A&A, 284, 749
Charlot, S., & Fall, S. M. 1993, ApJ, 415, 580
Davidge, T. J. 1989, PASP, 101, 494
Deharveng, J.-M., Buat, V., Le Brun, V., Milliard, B., Kunth, D., Shull, J. M., & Gry, C. 2001, A&A, 375, 805
Djorgovski, S., & Thompson, D. J. 1992, IAU Symp. 149, The Stellar Population of Galaxies, ed. B. Barbuy & A. Renzini (Dordrecht: Kluwer), 337
Frye, B., Broadhurst, T., & Benítez, N. 2002, ApJ, 568, 558
González Delgado, R. M., Leitherer, C., Heckman, T., Lowenthal, J. D., Ferguson, H. C., & Robert, C. 1998, ApJ, 495, 698
Hartmann, L. W., Huchra, J. P., Geller, M. J., O'Brien, P., & Wilson, R. 1988, ApJ, 326, 101
Heckman, T. M. 2001, ASP Conf. Ser. 240, Gas and Galaxy Evolution, ed. J. E. Hibbard, M. P. Rupen, & J. H. van Gorkum (San Francisco: ASP), 345
Heckman, T. M., Sembach, K. R., Meurer, G. R., Leitherer, C., Calzetti, D., & Martin, C. L. 2001, ApJ, 558, 56
Hurwitz, M., Jelinsky, P., & Dixon, W. V. D. 1997, ApJ, 481, L31
Kennicutt, R. C., Kobulnicky, H. A., & Pizagno, J. L. 1998, BAAS, 30, 1354
Kudritzki, R.-P. et al. 2000, ApJ, 536, 19
Kunth, D., Leitherer, C., Östlin, G., Mas-Hesse, J. M, Petrosian, A. 2003, ApJ, 577, 263
Kunth, D., Lequeux, J., Sargent, W. L. W., & Viallefond, F. 1994, A&A, 282, 709
Kunth, D., Mas-Hesse, J. M., Terlevich, E., Terlevich, R., Lequeux, J., & Fall, S. M. 1998, A&A, 334, 11
Legrand, F., Kunth, D., Mas-Hesse, J. M., & Lequeux, J. 1997, A&A, 326, 929
Leitherer, C., Ferguson, H. C., Heckman, T. M., & Lowenthal, J. D. 1995, ApJ, 454, L19
Lequeux, J., Kunth, D., Mas-Hesse, J. M., & Sargent, W. L. W. 1995, A&A, 301, 18
Maíz-Apellániz, J., Mas-Hesse, J. M., Muñoz-Tuñón, C., Vílchez, J. M., & Castañeda, H. O. 1998, A&A, 329, 409
Mar, D. P., & Bailey, G. 1995, Proc. Astron. Soc. Australia, 12, 239
Margon, B., Anderson, S. F., Mateo, M., Fich, M., & Massey, P. 1988, ApJ, 334, 597
Martin, C. L. 1996, ApJ, 465, 680
Mas-Hesse, J. M., & Kunth D. 1999, A&A, 349, 765
Meier, D. L., & Terlevich, R. 1981, ApJ, 246, L109
Melnick, J., Terlevich, R., & Terlevich, E. 2000, MNRAS, 311, 629
Neufeld, D. A. 1990, ApJ, 350, 216
Pagel, B. E. J., Simonson, E. A., Terlevich, R. J., & Edmunds, M. G. 1992, MNRAS, 255, 325
Partridge, R. B., & Peebles, P. J. E. 1967, ApJ, 148, 377
Pettini et al. 2000, ApJ, 528, 96
———. 2001, ApJ, 554, 981
Rhoads, J. E., Malhotra, S., Dey, A., Stern, D., Spinrad, H., & Jannuzi, B. T. 2000, ApJ, 545, L85
Schaerer, D. 2002, A&A, 382, 28
Shapley, A. E., Steidel, C. C., Adelberger, K. L., Dickinson, M., Giavalisco, M., & Pettini, M. 2001, ApJ, 562, 95
Shapley, A. E., Steidel, C. C., Pettini, M., & Adelberger, K. L. 2003, ApJ, 588, 65
Shull, J. M., & Silk, J. 1979, ApJ, 234, 427
Skillman, E. D., & Kennicutt, R. C. 1993, ApJ, 411, 655
Steidel, C. C., Adelberger, K. L., Giavalisco, M., Dickinson, M., & Pettini, M. 1999, ApJ, 519, 1
Steidel, C. C., Pettini, M., & Adelberger, K. L. 2001, ApJ, 546, 665
Tenorio-Tagle, G., Silich, S. A., Kunth, D., Terlevich, E., & Terlevich, R. 1999, MNRAS, 309, 332
Terlevich, E., Díaz, A. I., Terlevich, R., & Vargas, M. L. G. 1993, MNRAS, 260, 3
Thuan, T. X., & Izotov, Y. I. 1997, ApJ, 489, 623
Thuan, T. X., Izotov, Y. I., & Lipovetsky, V. A. 1997, ApJ, 477, 661
Valls-Gabaud, D. 1993, ApJ, 419, 7